

Strong temperature gradients in the ice age North Atlantic Ocean revealed by plankton biogeography

Received: 24 May 2023

Accepted: 19 October 2023

Published online: 5 December 2023

 Check for updates

Lukas Jonkers¹✉, Thomas Laepple^{1,2,3}, Marina C. Rillo^{1,4}, Xiaoxu Shi^{5,6}, Andrew M. Dolman², Gerrit Lohmann^{1,5}, André Paul¹, Alan Mix⁷ & Michal Kucera^{1,3}

The cold Last Glacial Maximum, around 20,000 years ago, provides a useful test case for evaluating whether climate models can simulate climate states distinct from the present. However, because of the indirect and uncertain nature of reconstructions of past environmental variables such as sea surface temperature, such evaluation remains ambiguous. Instead, here we evaluate simulations of Last Glacial Maximum climate by relying on the fundamental macroecological principle of decreasing community similarity with increasing thermal distance. Our analysis of planktonic foraminifera species assemblages from 647 sites reveals that the similarity-decay pattern that we obtain when the simulated ice age seawater temperatures are confronted with species assemblages from that time differs from the modern. This inconsistency between the modern temperature dependence of plankton species turnover and the simulations arises because the simulations show globally rather uniform cooling for the Last Glacial Maximum, whereas the species assemblages indicate stronger cooling in the subpolar North Atlantic. The implied steeper thermal gradient in the North Atlantic is more consistent with climate model simulations with a reduced Atlantic meridional overturning circulation. Our approach demonstrates that macroecology can be used to robustly diagnose simulations of past climate and highlights the challenge of correctly resolving the spatial imprint of global change in climate models.

Earth's climate was fundamentally different from today during the Last Glacial Maximum (LGM; 23,000–19,000 years ago). Atmospheric carbon dioxide concentration was much lower, at approximately 185 ppm (ref. 1), large ice sheets covered northern North America and Eurasia² and ocean circulation was different³. Since anthropogenic climate

change is projected to shift the climate system towards a different state⁴, it is essential to evaluate the performance of climate models under boundary conditions different from today⁵. Simulation of LGM climate has therefore been key to evaluate climate models^{6–8}. Decades of data–model comparison have shown that the overall change in global

¹MARUM Center for Marine Environmental Sciences, University of Bremen, Bremen, Germany. ²Alfred-Wegener-Institut, Helmholtz-Zentrum für Polar- und Meeresforschung, Potsdam, Germany. ³Department of Geosciences, University of Bremen, Bremen, Germany. ⁴Institute for Chemistry and Biology of Marine Environments, Carl-von-Ossietzky University Oldenburg, Wilhelmshaven, Germany. ⁵Alfred-Wegener-Institut, Helmholtz-Zentrum für Polar- und Meeresforschung, Bremerhaven, Germany. ⁶Southern Marine Science and Engineering Guangdong Laboratory (Zhuhai), Zhuhai, China. ⁷College of Earth, Ocean, and Atmospheric Sciences, Oregon State University, Corvallis, OR, USA. ✉e-mail: ljonkers@marum.de

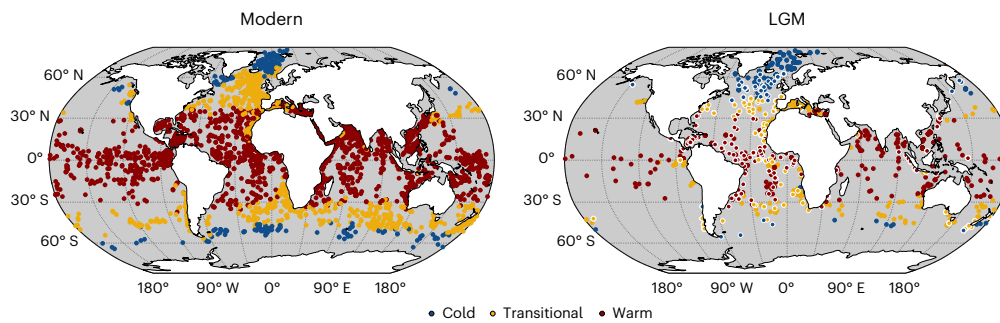


Fig. 1 | Planktonic foraminifera biogeography today (based on core-top data) and during the LGM. The species assemblages separated into three clusters (Methods) show a clear latitudinal pattern due to the influence of temperature on planktonic foraminifera species distribution. During the LGM, polar assemblages expanded further towards the Equator than today. This change occurred at the expense of transitional assemblages, whereas the extent of tropical assemblages

changed only marginally. This major reorganization of the foraminifera communities indicates a steepening meridional ecological gradient that was particularly pronounced in the North Atlantic Ocean. White rings around the dots in the right panel indicate sites added to previous work¹¹; all data sources are provided in Methods. Basemap from Natural Earth (<https://www.naturalearthdata.com/>).

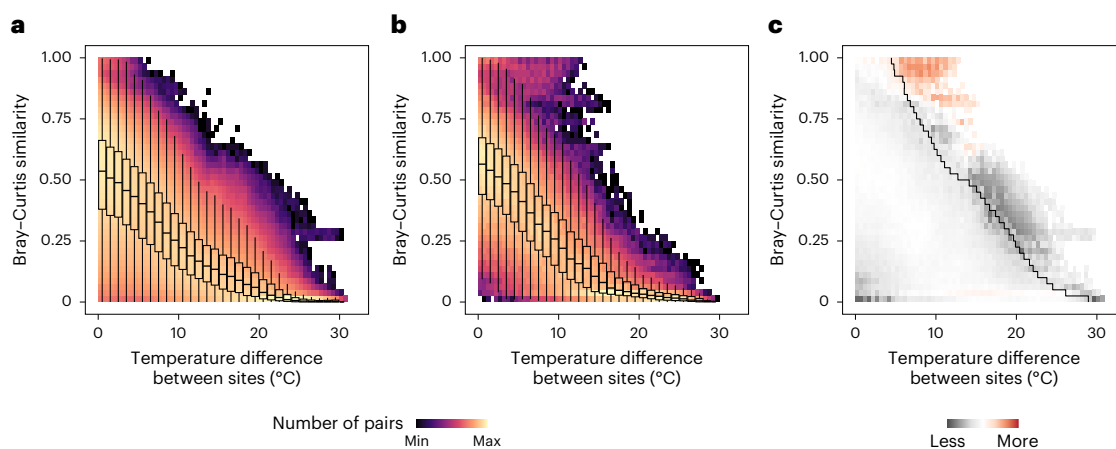


Fig. 2 | Simulated LGM temperature gradients are inconsistent with foraminifera biogeography. **a**, Modern. **b**, LGM. **c**, Difference. The core-top data (**a**) indicate that the similarity between assemblages decreases with increasing temperature difference. The box-plots indicate the median and interquartile range of the similarity; the whiskers extend to 1.5 times this range. They are shown at 1 °C bins, and heatmaps in the background show the normalized number of site pairs. The modern pattern (**a**) also appears when the LGM assemblages

are combined with simulated temperatures (**b**; ensemble mean). However, the simulations also show large temperature differences among some sites even though they have highly similar (>0.75) assemblages (**b**; and highlighted in red in **c**). Notably, these simulated temperature differences appear to lie outside the modern limits for assemblages as shown by the black step line in **c**, which depicts the 99th percentile of thermal distance as a function of similarity. All data sources are provided in Methods.

climate between the LGM and the present is consistent among models and palaeoclimate reconstructions, but ambiguities remain in the spatial pattern of glacial cooling^{8–11}. This is problematic because the spatial temperature pattern is of fundamental importance for climate dynamics and also governs the distribution of habitats and ecosystems on our planet.

Assessing climate model performance using palaeoclimate reconstructions is, however, intrinsically challenging because the indirect nature of the reconstructions renders it difficult to determine whether differences between reconstructions and simulations reflect poor model skill or ambiguity in the proxy data^{12,13}. In seawater temperature reconstructions, ambiguity arises from uncertainty in the attribution of the temperature signal to the depth and season where it originated and from the effect of nuisance parameters confounding the otherwise dominant effect of temperature on the proxy^{14,15}. Simulations, on the other hand, are also associated with ambiguity due to model set-up, experimental design and structural uncertainty. Thus, the attribution of the differences between reconstructions and simulations to either the proxy data or the models is challenging and calls for alternative ways to evaluate simulations of past climate.

The first global reconstruction of LGM temperatures used transfer functions that relate (marine) microfossil assemblage composition to (seawater) temperature¹⁶. Since then, new geochemical methods to reconstruct past temperature have become available, but the transfer-function approach still is an important tool in palaeoclimatology^{17,18}. However, in theory, species assemblage data could also provide a direct way to evaluate climate models independently of the reconstructed temperatures. Differences in habitat preferences among species result in changes in assemblage composition along ecologically relevant environmental gradients¹⁹. Thus, the compositional similarity between assemblages decreases the further apart they are from each other in the environmental space. Such similarity decay is a fundamental concept in ecology and is observed in many different taxa and ecosystems^{20,21}. Like in other marine organisms²², temperature has consistently been shown to be the main driver of community assembly in planktonic foraminifera on a global scale^{23,24} (Fig. 1). Indeed, modern planktonic foraminifera assemblages from core-top sediments show a strong monotonic decrease in compositional similarity with increasing temperature difference (Fig. 2a). Contrary to phytoplankton, planktonic foraminifera assemblages

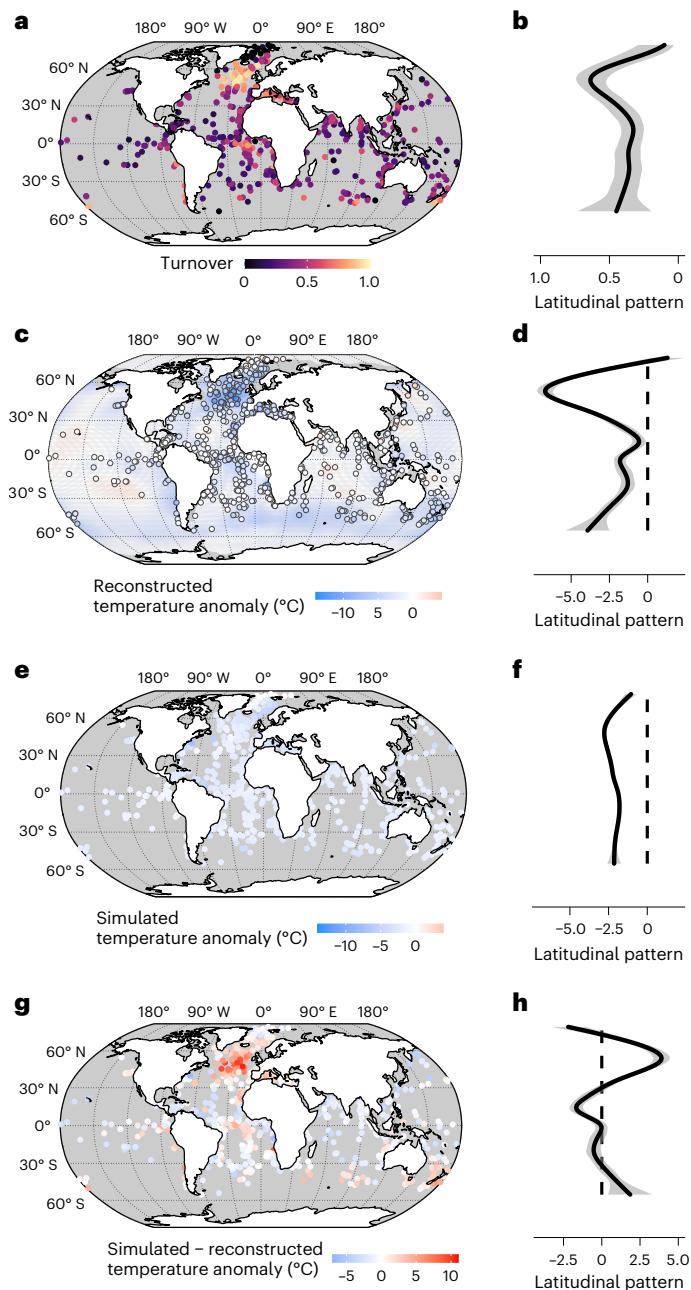


Fig. 3 | Large model–data differences during the LGM in areas of marked species turnover. **a–d**, The large temporal turnover in planktonic foraminifera assemblages in the North Atlantic (**a**, **b**) is consistent with a pronounced cooling (**c**, **d**; background in **c** shows gridded reconstruction; Methods). **e–h**, The simulations, by contrast, show globally rather uniform cooling (**e**, **f**), and appear too warm in the North Atlantic (**g**, **h**). Simulated temperature and the model–data difference (**e**, **g**; ensemble mean) are shown only at the locations where data are available. **b**, **d**, **f**, **h**, The latitudinal pattern smoothed using a generalized additive model, with the 95% confidence interval in grey. Data sources are provided in Methods. Basemaps in **a**, **c**, **e**, **g** from Natural Earth (<https://www.naturalearthdata.com/>).

have changed consistently with recurrent glacial–interglacial cycles over the late Quaternary period²⁵. Given low dispersal limitations in the marine realm compared with on land, this consistent glacial–interglacial change demonstrates that planktonic foraminifera species have tracked climate change, that is, that their thermal niches have remained stable^{26,27} rather than (evolutionarily) adapted to the changing climate. Because of this stability of the thermal niches of planktonic

foraminifera, the similarity–decay pattern observed in the core–top data should also characterize past assemblages. Thus, comparison of the similarity–decay pattern obtained using fossil species assemblages and simulated temperatures against the reference pattern seen in the core–top data offers an alternative way to evaluate climate models that is firmly grounded on ecological principles. This approach allows a direct comparison of observations and simulations, and hence does not rely on space–for–time substitution that is used for the calibration of temperature proxies, because it is based on the relationship between spatial gradients in species composition and in temperature. Moreover, this approach makes full use of the data, as gradients are assessed in all directions rather than in a point–by–point comparison. Finally, seasonal and vertical habitat tracking by planktonic foraminifera species, which complicates climate reconstructions based on their geochemistry²⁸, is implicitly accounted for in the method.

In this Article, we use a new dataset of 2,085 LGM planktonic foraminifera morphospecies assemblages from 647 unique sites (Fig. 1), which represents a 50% increase in coverage compared with previous work¹⁷ to apply this new macroecological approach. We evaluate near surface seawater temperature patterns from a suite of equilibrium simulations of LGM carried out using a common protocol with state-of-the-art climate models (Methods).

LGM plankton biodiversity patterns

Our new dataset shows clear differences in biogeography between modern and LGM planktonic foraminifera (Fig. 1). The largest change occurred in the North Atlantic Ocean, where cold-water assemblages expanded to the mid-latitudes at the expense of transitional fauna. Evidence that the changes in the assemblage composition reflect changes in the climate, rather than an adaptation of the ecological preferences of the foraminifera species, stems from the good compositional analogues of the LGM species assemblages for virtually all sites (98%; Methods). Adaptation—changes in the thermal niches—would result in different glacial species assemblages than seen today. Thus, the near absence of poor analogues provides further support for the assumption that the similarity–decay pattern observed in the core–top assemblages should also characterize those from the LGM. Hence, if the models simulate LGM cooling accurately, the similarity–decay pattern obtained using simulated temperatures should be indistinguishable from the core–top pattern.

To a first degree, the simulated temperatures indeed imply a similarity decay that is similar to that seen in the core–top data, suggesting that the global pattern of LGM seawater temperature is reasonably well simulated and that planktonic foraminifera changed their distribution consistent with their modern thermal preferences (Fig. 2). However, the LGM similarity–decay pattern obtained using simulated temperatures also shows clear differences from the core–top pattern (Fig. 2). The discrepancy is largest at high (>0.75) similarities, where in many cases the simulated temperature differences exceed the limits indicated by modern assemblages (Fig. 2). This pattern is a salient feature that characterizes all simulations (Extended Data Fig. 1) and is robust against chronological uncertainty (Methods and Extended Data Fig. 8). It arises mainly from the similarity among LGM plankton assemblages in the North Atlantic and the Nordic Seas (Extended Data Fig. 2), where the models maintain the large present-day temperature gradient. This anomalous LGM pattern does not reflect model bias, since the core–top similarity–decay pattern is reproduced with simulated temperatures from the pre-industrial control runs (Extended Data Fig. 3). Notably, the same pattern also appears when LGM similarities are plotted against present-day temperature differences (Extended Data Fig. 4). Thus, whereas the species assemblages indicate changes in the spatial temperature gradients in the LGM, the simulated cooling appears globally rather uniform, without marked changes in oceanic thermal gradients. The distribution of foraminifera during the LGM and the modelled LGM temperatures therefore appear incompatible.

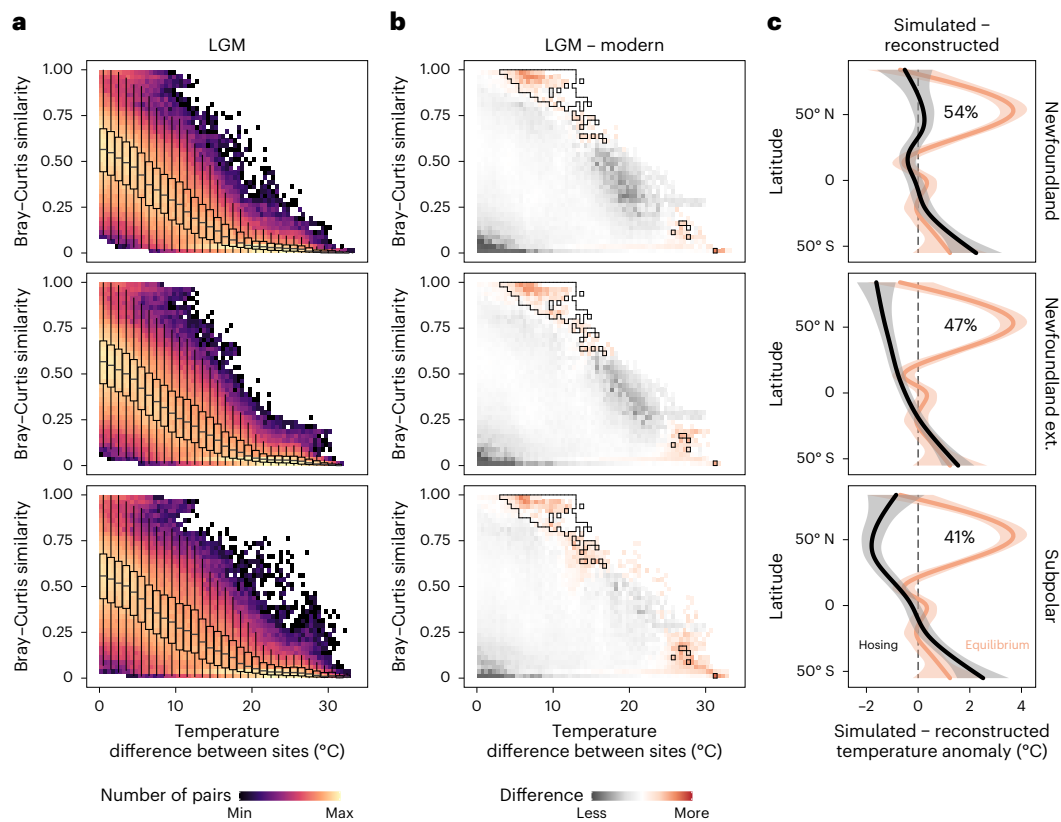


Fig. 4 | Simulations with a colder North Atlantic improve data-model agreement. **a, b**, The LGM similarity-decay patterns based on temperatures from the simulation with freshwater input into the North Atlantic (**a**) are more similar to the modern pattern (**b**) as the number of site pairs with high similarity, but large temperature difference between them, is reduced compared with the equilibrium simulation (symbols in panel **a** as in Fig. 2; black lines in **b** delineate the areas with excess temperature differences between sites in the equilibrium simulation; Extended Data Fig. 1). **c**, The difference between the simulated and

reconstructed temperatures (black) is also reduced compared to the equilibrium simulations (red). Percentages in **c** indicate reduction in difference in the subpolar North Atlantic. Lines show the meridional pattern, approximated using a generalized additive model smooth, with the 95% confidence interval indicated. The results are presented for the different experiments where the freshwater flux was applied to either offshore Newfoundland or the subpolar North Atlantic. In the extended experiment (Newfoundland ext.), the forcing was applied for 1,050 years instead of 150. Details and the data sources are provided in Methods.

There is no evidence for the emergence of new species or traits or for species extinctions since the LGM²⁹, which is consistent with the good compositional analogues between the present and the LGM (Methods). Moreover, there is no indication for a widening of the thermal niche of cold-water species that expanded into the mid-latitude North Atlantic (Fig. 1). Such adaptation would allow those species to migrate into areas with temperatures warmer than their current thermal range but would result in geochemistry-based estimates of LGM temperature that are warmer than present. However, such positive temperature anomalies are very rare in the most recent compilation of LGM seawater temperature proxies³⁰. We therefore rule out that the relationship between planktonic foraminifera ecology and temperature has changed on the studied timescale. The good compositional analogues also argue against the existence of presently unobserved oceanic conditions during the LGM. Thus, although there is, in theory, the possibility that the relationship between temperature and assemblage composition arises from collinearity with another environmental variable, it is unlikely that this collinearity has changed globally in a systematic way. We are therefore left with the observation that the simulated LGM temperature change cannot explain fundamental biogeographic patterns in planktonic foraminifera that inhabited the ocean at that time.

Pronounced cooling in the glacial North Atlantic Ocean

To further assess the mismatch between the simulations and the foraminifera data, we estimate LGM temperatures from the

assemblages. We use a new approach to resolve ambiguities in the seasonal and vertical origin of the proxy signal that have hindered previous comparisons of this kind (Methods). We find that, globally, planktonic foraminifera assemblages best reflect annual seawater temperatures at 50 m water depth. Averaged across the sites, the resulting reconstructed temperatures of LGM seawater (Fig. 3) are 2.45 °C (2.33–2.57 °C; 95% confidence interval) lower than today. The simulations show a similar degree of cooling (–1.30 to –2.89 °C, ensemble mean –2.15 °C), indicating reasonable agreement on a global scale and testifying to the stability of the thermal niches of planktonic foraminifera since the LGM.

However, these averaged values of temperature change hide marked differences in the spatial pattern of LGM cooling. The replacement of transitional assemblages with cold-water assemblages in the North Atlantic (Figs. 2 and 3) is associated with large-scale cooling. Reconstructed subpolar North Atlantic (40°–60° N) temperatures are on average 7.3 °C lower than today, leading to drastically different meridional temperature gradients (Extended Data Fig. 5). By contrast, simulated temperature anomalies are spatially rather uniform, and the North Atlantic cooling is markedly weaker in all simulations we assessed (Fig. 3). Differences between the simulations and the reconstructions reach up to 4.9 °C averaged across the North Atlantic (40°–60° N; ensemble mean and up to 8.3 °C for individual models; Extended Data Fig. 5), far beyond the uncertainty of the reconstructions (Methods).

The data thus indicate a marked reorganization of the North Atlantic oceanography. The spatial pattern of the temporal species

turnover and reconstructed temperature change (Fig. 3) resembles the fingerprint of the Atlantic meridional overturning circulation (AMOC). AMOC changes can create such a characteristic temperature anomaly through changes in the location of deep convection and the subpolar gyre circulation³¹. A weaker glacial AMOC, or reduction in its northward extent, is thus a conceivable explanation for the discrepancy. To test this hypothesis, we investigated additional simulations with one of the models under identical LGM boundary conditions but with a weaker AMOC than in the LGM equilibrium simulations (Methods). These experiments yield an ocean that is in closer agreement with the biogeography of planktonic foraminifera. The additional three simulations are characterized by a colder subpolar North Atlantic, which results in similarity-decay patterns that are in closer agreement with the core-top pattern (Fig. 4a,b). Differences between reconstructed and simulated temperatures are also reduced in the experiments with a weaker AMOC, especially in the mid-latitude North Atlantic, where the reduction reaches up to approximately 50% (Fig. 4c and Extended Data Fig. 6). Thus, the representation of the AMOC in the equilibrium simulations appears a likely source of the discrepancy between the observations and the simulations.

In these experiments, the reduction in the AMOC was achieved by prescribing freshwater flux into the North Atlantic Ocean. In two experiments, a 150 yr, 0.2 Sv freshwater forcing was applied to either offshore Newfoundland or the central subpolar North Atlantic³², with the latter showing a larger reduction in the AMOC and stronger associated cooling. To assess the ocean response to forcing that is (more) commensurate with the duration of the LGM, we conducted a third experiment, in which we applied a stochastically varying freshwater flux (0.1 ± 0.05 Sv) near the coast of Newfoundland for 1,050 years, simulating persistent, but variable discharge from the Laurentide ice sheet. In all experiments, the AMOC shows a marked slowdown (coastal: 11.8 Sv; subpolar: 4.3 Sv; coastal long: 8.1 Sv), which appears in closer agreement with reconstructions of deep ocean circulation^{33,34} compared with the default LGM simulation (18.2 Sv).

Our experiments were designed to mimic freshwater input by ice-sheet melting and calving as we hypothesize that the large ice sheets during the LGM may have been in a dynamic equilibrium with local stochastic mass loss similar to continental ice sheets today³⁵. However, cooling in the North Atlantic can in simulations also result from other processes such as changes in the ice-sheet height or in oceanic mixing^{36,37}. Nevertheless, the additional experiments demonstrate that a reduced AMOC is a physically plausible mechanism to bring the reconstructions and simulations in closer agreement.

By combining insights from different disciplines, we have demonstrated the power of using ecological principles to evaluate simulations of past climate. Because similarity decay with temperature arises from the strong temperature dependence of planktonic foraminifera species distribution, the method used here can, in principle, also be applied to assemblages containing extinct species, providing new ways to assess simulations of climate in the distant past. Our analysis indicates distinct regional patterns in the LGM temperature change, with the largest cooling in the northern North Atlantic, probably related to a markedly reduced AMOC. Resolving the changes in the oceanic thermal gradients indicated by planktonic foraminifera assemblages is a clear target for simulations, including transient ones, of LGM climate. Finally, the spatial heterogeneity of climate change that is robustly implied by glacial plankton biogeography underscores the need for climate model evaluation beyond globally averaged statistics since the spatial heterogeneity of climate change is critical for ecosystems and our society.

Online content

Any methods, additional references, Nature Portfolio reporting summaries, source data, extended data, supplementary information, acknowledgements, peer review information; details of author contributions

and competing interests; and statements of data and code availability are available at <https://doi.org/10.1038/s41561-023-01328-7>.

References

- Monnin, E. et al. Atmospheric CO₂ concentrations over the Last Glacial Termination. *Science* **291**, 112–114 (2001).
- Clark, P. U. & Mix, A. C. Ice sheets and sea level of the Last Glacial Maximum. *Quat. Sci. Rev.* **21**, 1–7 (2002).
- Lippold, J. et al. Strength and geometry of the glacial Atlantic meridional overturning circulation. *Nat. Geosci.* **5**, 813–816 (2012).
- IPCC *Climate Change 2021: The Physical Science Basis* (eds Masson-Delmotte, V. et al.) (Cambridge Univ. Press, 2021).
- Tierney, J. E. et al. Past climates inform our future. *Science* **370**, eaay3701 (2020).
- Schmidt, G. A. et al. Using palaeo-climate comparisons to constrain future projections in CMIP5. *Clim. Past* **10**, 221–250 (2014).
- Manabe, S. & Hahn, D. G. Simulation of the tropical climate of an ice age. *J. Geophys. Res.* **82**, 3889–3911 (1977).
- Kageyama, M. et al. The PMIP4 Last Glacial Maximum experiments: preliminary results and comparison with the PMIP3 simulations. *Clim. Past* **17**, 1065–1089 (2021).
- Braconnot, P. et al. Evaluation of climate models using palaeoclimatic data. *Nat. Clim. Change* **2**, 417–424 (2012).
- Harrison, S. P. et al. Evaluation of CMIP5 palaeo-simulations to improve climate projections. *Nat. Clim. Change* **5**, 735–743 (2015).
- MARGO Project Members. Constraints on the magnitude and patterns of ocean cooling at the Last Glacial Maximum. *Nat. Geosci.* **2**, 127–132 (2009).
- Lohmann, G., Pfeiffer, M., Laepple, T., Leduc, G. & Kim, J.-H. A model–data comparison of the Holocene global sea surface temperature evolution. *Clim. Past* **9**, 1807–1839 (2013).
- Reschke, M., Kröner, I. & Laepple, T. Testing the consistency of Holocene and Last Glacial Maximum spatial correlations in temperature proxy records. *J. Quat. Sci.* **36**, 20–28 (2021).
- Telford, R. J., Li, C. & Kucera, M. Mismatch between the depth habitat of planktonic foraminifera and the calibration depth of SST transfer functions may bias reconstructions. *Clim. Past* **9**, 859–870 (2013).
- Jonkers, L. & Kučera, M. Sensitivity to species selection indicates the effect of nuisance variables on marine microfossil transfer functions. *Clim. Past* **15**, 881–891 (2019).
- CLIMAP Project Members. The surface of the ice-age Earth. *Science* **191**, 1131–1137 (1976).
- Kucera, M. et al. Reconstruction of sea-surface temperatures from assemblages of planktonic foraminifera: multi-technique approach based on geographically constrained calibration data sets and its application to glacial Atlantic and Pacific Oceans. *Quat. Sci. Rev.* **24**, 951–998 (2005).
- Marsicek, J., Shuman, B. N., Bartlein, P. J., Shafer, S. L. & Brewer, S. Reconciling divergent trends and millennial variations in Holocene temperatures. *Nature* **554**, 92–96 (2018).
- Chase, J. M. Spatial scale resolves the niche versus neutral theory debate. *J. Veg. Sci.* **25**, 319–322 (2014).
- Soininen, J., McDonald, R. & Hillebrand, H. The distance decay of similarity in ecological communities. *Ecography* **30**, 3–12 (2007).
- Graco-Roza, C. et al. Distance decay 2.0—a global synthesis of taxonomic and functional turnover in ecological communities. *Glob. Ecol. Biogeogr.* **31**, 1399–1421 (2022).
- Antão, L. H. et al. Temperature-related biodiversity change across temperate marine and terrestrial systems. *Nat. Ecol. Evol.* <https://doi.org/10.1038/s41559-020-1185-7> (2020).
- Morey, A. E., Mix, A. C. & Pisias, N. G. Planktonic foraminiferal assemblages preserved in surface sediments correspond to multiple environment variables. *Quat. Sci. Rev.* **24**, 925–950 (2005).

24. Rillo, M. C., Woolley, S. & Hillebrand, H. Drivers of global pre-industrial patterns of species turnover in planktonic foraminifera. *Ecography* <https://doi.org/10.1111/ecog.05892> (2021).
25. Peeters, F. J. C. et al. Vigorous exchange between the Indian and Atlantic oceans at the end of the past five glacial periods. *Nature* **430**, 661–665 (2004).
26. Antell, G. T., Fenton, I. S., Valdes, P. J. & Saupe, E. E. Thermal niches of planktonic foraminifera are static throughout glacial–interglacial climate change. *Proc. Natl Acad. Sci. USA*. **118**, e2017105118 (2021).
27. Dowsett, H. et al. The relative stability of planktic foraminifer thermal preferences over the past 3 million years. *Geosci. J.* **13**, 71 (2023).
28. Jonkers, L. & Kučera, M. Quantifying the effect of seasonal and vertical habitat tracking on planktonic foraminifera proxies. *Clim. Past* **13**, 573–586 (2017).
29. Kucera, M. & Schönfeld, J. in *Deep-Time Perspectives on Climate Change: Marrying the Signal from Computer Models and Biological Proxies* (eds Williams, M. et al.) 409–426 (Geological Society, 2007).
30. Tierney, J. E. et al. Glacial cooling and climate sensitivity revisited. *Nature* **584**, 569–573 (2020).
31. Caesar, L., Rahmstorf, S., Robinson, A., Feulner, G. & Saba, V. Observed fingerprint of a weakening Atlantic Ocean overturning circulation. *Nature* **556**, 191–196 (2018).
32. Lohmann, G., Butzin, M., Eissner, N., Shi, X. & Stepanek, C. Abrupt climate and weather changes across time scales. *Paleoceanogr. Paleoclimatol.* **35**, e2019PA003782 (2020).
33. Pöppelmeier, F., Jeltsch-Thömmes, A., Lippold, J., Joos, F. & Stocker, T. F. Multi-proxy constraints on Atlantic circulation dynamics since the last ice age. *Nat. Geosci.* **16**, 349–356 (2023).
34. Hesse, T., Butzin, M., Bickert, T. & Lohmann, G. A model–data comparison of $\delta^{13}\text{C}$ in the glacial Atlantic Ocean. *Paleoceanography* **26**, PA3220 (2011).
35. Enderlin, E. M. et al. An improved mass budget for the Greenland ice sheet. *Geophys. Res. Lett.* **41**, 866–872 (2014).
36. Sherriff-Tadano, S. & Abe-Ouchi, A. Roles of sea ice–surface wind feedback in maintaining the glacial Atlantic meridional overturning circulation and climate. *J. Clim.* **33**, 3001–3018 (2020).
37. Vettoretti, G. & Peltier, W. R. Last Glacial Maximum ice sheet impacts on North Atlantic climate variability: the importance of the sea ice lid. *Geophys. Res. Lett.* **40**, 6378–6383 (2013).

Publisher's note Springer Nature remains neutral with regard to jurisdictional claims in published maps and institutional affiliations.

Open Access This article is licensed under a Creative Commons Attribution 4.0 International License, which permits use, sharing, adaptation, distribution and reproduction in any medium or format, as long as you give appropriate credit to the original author(s) and the source, provide a link to the Creative Commons license, and indicate if changes were made. The images or other third party material in this article are included in the article's Creative Commons license, unless indicated otherwise in a credit line to the material. If material is not included in the article's Creative Commons license and your intended use is not permitted by statutory regulation or exceeds the permitted use, you will need to obtain permission directly from the copyright holder. To view a copy of this license, visit <http://creativecommons.org/licenses/by/4.0/>.

© The Author(s) 2023

Methods

Data

Planktonic foraminifera assemblages. To characterize the modern similarity-decay pattern and to calibrate the transfer-function models, we used core-top planktonic foraminifera assemblage data from the ForCenS compilation³⁸. This compilation contains species relative abundances based on counts of at least 300 specimens in the size fraction >150 μm . For some sites, the ForCenS compilation contains replicate counts, and as in previous work³⁹, we randomly preserved a single sample from those sites, resulting in a total of 3,916 samples from unique sites from across the global ocean.

For the LGM, we extended the multiproxy approach for the reconstruction of the glacial ocean surface (MARGO) compilation¹¹ by over 50% using identical criteria for inclusion to ensure compatibility. We compiled data from literature^{40–78} and added new samples from sediment cores with age control based on radiocarbon dating^{79–90}. Counts from the new samples were performed on aliquots containing at least 300 specimens in the size fraction >150 μm and following the ForCenS taxonomy³⁸. Our new dataset contains 2,085 samples from 647 unique sites (Fig. 1). All new samples were assigned a chronological confidence level that is consistent with MARGO⁹¹. The highest confidence level is assigned to age control on the basis of layer counting or on at least two radiometric dates within the 19,000–23,000 years BP interval. Level 2 indicates age control based on two bracketing radiometric age-control points within the 12,000–30,000 years BP interval or by correlation to regional records with level 1 chronology. Level 3 chronologies are based on other stratigraphic constraints correlated to records that match level 2. Data for which age control could no longer be verified, but were previously assigned to the LGM interval, are indicated with level 4. The taxonomically harmonized dataset includes extensive metadata to facilitate reuse. We encourage future users of the data to also acknowledge the original sources of the assemblage and age-control data.

Climatology. To assess the similarity decay in the core-top datasets, develop the transfer-function model and derive LGM temperature anomalies, we used climatology data from a 100-km-radius circle around each data point because sediment samples integrate the export flux of foraminifera over a similar area^{92,93}. We tested the applicability of transfer-function models for different seasons and depths (see the following) and deliberately used the World Ocean Atlas version 1998⁹⁴ to reduce the bias of the most recent global warming on our inferences¹⁷.

Simulations. We assessed the Palaeoclimate Modelling Intercomparison Project (PMIP) phase 3 and phase 4 simulations that were available at the time of analysis. In total, these were ten simulations from eight models that have LGM and pre-industrial runs: NCAR-CCSM4^{95,96}, CNRM-CMS^{97,98}, FGOALS-g2^{99,100}, GISS-E2-R^{101,102}, MIROC-ESM^{103,104}, MPI-ESM-P^{105,106}, MRI-CGCM3^{107,108} and AWI-ESM³². These simulations were all run using fixed ice sheets and without freshwater hosing in the North Atlantic as described in the respective PMIP protocols^{109,110}. From these, CCSM4 and GISS have two LGM physics ensemble members each. The AWI-ESM has a higher spatial horizontal resolution in the ocean of up to 30 km. We used the potential temperature (θ) fields from the ocean models, and all data files have been remapped from their generic to a $1^\circ \times 1^\circ$ longitude–latitude grid using bilinear remapping. To ensure completeness of the temperature profiles, we created a common mask of existing data in the LGM and pre-industrial simulations at 100 m water depth for each simulation. From this mask of existing data, the nearest (in geometrical distance) gridbox containing the site was extracted. If the 50 m depth level was not in the model, the value was linearly interpolated from the existing depth levels.

We also compared our reconstructions with three experiments run using the AWI-ESM using the same LGM boundary conditions but with differing freshwater fluxes applied to the North Atlantic. In two

previously published experiments, a 0.2 Sv freshwater flux was applied 150 years³². These simulations differ in the location of the freshwater input: either between 50° and 70° N off the coast of Newfoundland close to the Labrador Sea (called Newfoundland in Fig. 4) or equally distributed across the same latitude band in the North Atlantic (called subpolar). A global conservation in salinity was enforced at each time step by subtracting the global mean changes in net water flux from the first ocean layer. In a third, new experiment, we applied a stochastically varying freshwater flux (0.1 ± 0.05 Sv) for 1,050 years in the same area off Newfoundland as in the other experiments (Newfoundland ext. in Fig. 4). For a more realistic representation of the freshwater impacts, we switched off the salinity conservation in this simulation and allowed the global mean salinity to decrease with the continuous input of freshwater. In all experiments, the reduction in the AMOC happens within 100 years. From the short experiments, we use the temperature fields averaged across the years 101–150 of the freshwater perturbation, and for the longer experiment we used values averaged over the last 250 years of the simulation.

Biodiversity patterns

We assessed biodiversity patterns using globally harmonized taxonomy in which both subspecies of *Globigerinoides ruber* and *Globorotalia menardii* and *Globorotalia tumida* were lumped because they were not always separated in our data. We first assessed whether the LGM assemblages are compositionally similar to the modern assemblages by comparing the dissimilarity (square chord distance) between the LGM assemblages and their most similar modern counterparts with a baseline established from the core-top assemblages. Following previous work¹¹¹, we used the fifth percentile of the pairwise dissimilarities in the global core-top dataset as a cut-off for poor analogues. The median minimum square chord distance between the LGM and the core-top assemblages is 0.09, and at 98% of the sites, the assemblages have a distance below the poor analogue threshold. This high similarity between the core-top and LGM assemblages provides strong evidence against changes in the environmental niches of the individual foraminifera species as well as against the existence of presently unseen oceanographic conditions during the LGM. It also warrants merging of the two datasets to visualize changes in planktonic foraminifera biogeography. To this end, we performed k-mean cluster analysis to identify changes in the distribution of cold-water, transitional and warm-water assemblages in the merged dataset (Fig. 1).

To investigate the similarity decay, we used the Bray–Curtis dissimilarity¹¹² because this metric is sensitive to small changes in assemblage composition and has been shown to yield robust characterizations of beta diversity¹¹³. The Bray–Curtis dissimilarity accounts for differences in the relative proportions of taxa, and we express similarity as $1 - \text{dissimilarity}$. To plot assemblage similarity as a function of environmental (temperature) distance (similarity or distance-decay plot), we used annual-mean temperature data at 50 m water depth.

We averaged LGM assemblages from the same sites before calculating the dissimilarities to avoid skewing the decay pattern towards higher similarity at zero thermal distance induced by replicate samples. To determine the LGM distance decay, we derived LGM temperatures from the simulated temperature anomaly to minimize possible model-specific bias. For the calculation of temporal turnover (Fig. 3), we used only LGM samples that have a core top within a 100 km radius to reduce turnover that is due to spatial, rather than temporal, compositional change. This cut-off distance is warranted by the fact that sediment samples spatially integrate over considerable distances⁹².

To assess the effect of differential spatial sampling of the core-top and LGM datasets on the similarity-decay pattern, we subsampled the core-top dataset to sites within a 100 km radius from the LGM samples and to the sites nearest to the LGM samples. The decay patterns of the subsampled data are nearly identical to the pattern using all core-top samples (Extended Data Fig. 7). Hence, we conclude that our reference

core-top similarity-decay pattern is not affected by differential sampling of the temperature gradient.

The anomalously high similarities among LGM assemblages at large simulated temperature differences do not arise from chronological uncertainty (Extended Data Fig. 8). They are present in all four subsets of the data, except in the subset with lowest chronological confidence (level 3) because of the spatial distribution of the samples. Notably, the thermal limits for differences between assemblages derived from the core-top data (black step(ped) line in Fig. 1) already incorporate noise due to chronological uncertainty in the data³⁹ and hence represent conservative estimates of the position of these limits. The fact that some simulated temperature differences fall outside these limits thus underscores the chronological robustness of our findings.

To evaluate whether the anomalous LGM similarity-decay pattern reflects model-specific bias or arises from the LGM simulations, we compared the climatology-derived core-top similarity-decay pattern with the patterns obtained using the (pre-industrial) control runs of the climate models. The patterns obtained using simulated temperatures show only minor differences from those obtained using climatology and, importantly, do not show the excess similarities at large temperature differences (Extended Data Fig. 3). Thus, the odd pattern in the LGM similarity decay is a phenomenon related to the way glacial conditions are simulated. At the same time, these results suggest that the similarity-decay pattern in the core-top data is not due to post-industrial changes in temperature gradients, consistent with the globally uniform nature of anthropogenic warming¹⁴.

Finally, the difference between the modern similarity-decay pattern and the simulation-based LGM pattern could in theory also arise from some degree of ecological noise in the assemblage data. We note, however, that the cluster of site pairs with anomalously large temperature differences at high similarity lies outside the limits of the modern decay pattern (Fig. 2). Moreover, the difference in the decay patterns originates from the North Atlantic, where the strength of the modern similarity–temperature relationship is larger (pseudo r^2 : 0.71) than the global average (pseudo r^2 : 0.47). Here the pseudo r^2 is calculated as $1 - \left(\frac{\text{model deviance}}{\text{null deviance}} \right)$ derived from a binomial generalized linear model with a log link to account for the nonlinear nature of the data. We therefore conclude that the difference between the modern decay pattern and the LGM decay pattern using simulated temperatures is robust.

Temperature estimates

Previous work has documented that temperature is the single best predictor of planktonic foraminifera species assemblage composition on a global scale^{23,115}, and various transfer-function techniques have been successfully applied to obtain temperature estimates of the past ocean¹⁷. Here we use the modern analogue technique to derive temperature estimates from the species assemblages because this method is conceptually simple and allows for nonlinearity in the response of planktonic foraminifera assemblages. We develop transfer-function models for individual regions to minimize the effect of endemism of cryptic species, which has been shown to negatively impact transfer-function performance¹⁷. Regions were defined as in previous work¹⁷, and the taxonomy was harmonized to retain as many samples possible in each region. Specifically, this means that for the Mediterranean, the subspecies of *Globigerinoides ruber* were lumped and that *Globorotalia menardii* and *Globorotalia tumida* were combined in the Pacific. Temperature estimates were based on the similarity weighted mean of the ten best analogues, and analogue quality was assessed using the squared chord distance because this metric has been shown to be most effective in identifying analogues in microfossil datasets¹¹⁶.

Vertical and seasonal attribution. In contrast to previous work, we provide temperature reconstructions for a single season only. This is because seasonal seawater temperatures are highly correlated, and temperatures at different seasons have therefore little, if any,

independent predictive power^{17,23,117}. This issue has been touched upon before¹⁷, and here we make the conscious decision to break with convention and provide only a single independent estimate of past temperature. However, ambiguity persists as to which seasonal temperature the species assemblages reflect best¹⁴. Given the three-dimensional nature of the ocean, the same applies to the vertical dimension because planktonic foraminifera have not only variable seasonal abundances¹¹⁸ but also variable depth habitats in the global ocean¹¹⁹. We address this problem by estimating the proportion of variance in the species assemblages that is explained by temperature during different seasons and at different depths^{14,117}. The temperature during the season and at the depth that explains globally most of the variance in the species assemblages is then used for the final transfer-function model that is applied to estimate temperature from the fossil samples.

We first performed this analysis using canonical correspondence analysis on the core-top assemblages data using temperatures from climatology as constraining variables. Then to test the significance of temperature estimates from transfer functions, we also evaluated to what degree the temperatures predicted from both the core-top and the LGM assemblages explain the variance in the assemblages themselves. In doing so, we extended the framework used to assess significance of transfer-function predictions in previous work^{14,117} from the temporal to the spatial domain. We derived the proportion of variance in the first principal component of the assemblage data that is explained by the predicted temperatures assuming that this first component captures the imprint of the environmental variability (in space) on the assemblage data.

We assessed four seasons and annual mean at 14 different depth levels in the upper 500 m for five regions; that is, we built 350 transfer-function models to derive temperature estimates for the modern and fossil dataset. Given the larger vertical than seasonal temperature gradients in the tropics²⁸, we analysed tropical and extratropical regions separately. Irrespective of whether we assessed core-top or LGM assemblages, we found that seasonal temperatures explain nearly the same amount of variance in the species assemblages in most regions and that the choice of seasonal temperature for transfer-function development is not critical (Extended Data Fig. 9). A different picture emerges when considering depth. Especially in the tropics, there is a clear pattern in the depth at which temperature explains most of the variance; outside of the tropics, the dependence on depth is markedly smaller (Extended Data Fig. 9). Although there are regional differences, the tropics generally show a maximum in the explained variance that is not at, but slightly below, the sea surface. Globally, most of the variance in the modern as well as in the fossil planktonic foraminifera assemblages is explained by mean annual temperatures at 50 m water depth. We thus estimated LGM temperatures using the transfer-function model trained on annual-mean temperatures at 50 m water depth.

Negligible effect of poor analogues. A potential caveat with the use of transfer functions is the presence of fossil samples with low similarity to the samples in the modern training set, the so-called poor analogue problem. Warm LGM subtropical gyres, a consistent feature of planktonic foraminifera assemblage-based seawater temperature reconstructions^{16,17}, have previously been attributed to poor analogues. To some degree, this problem can be related to the species assemblage variability captured in the training set. Compared with previous work, we used a much more extensive core-top dataset, and we thus expect the poor analogue problem to be smaller. Nevertheless, to assess the possible effect on the reconstructed temperature of LGM assemblages that lack close analogues in the core-top dataset, we filtered out samples with a minimum square chord distance to the core-top samples above the fifth percentile of the pairwise dissimilarities in the global core-top dataset¹¹¹ (Extended Data Fig. 10). The mean

and 95 percentile range of the reconstruction are $-2.45\text{ }^{\circ}\text{C}$ (-9.51 to $1.22\text{ }^{\circ}\text{C}$) without analogue filtering. Global analogue filtering reduces the number of samples and sites by 169 and 15, respectively, and yields a mean temperature change of $-2.46\text{ }^{\circ}\text{C}$ (-9.55 to $1.27\text{ }^{\circ}\text{C}$). When using a regionally defined threshold, the dataset is reduced by 252 samples and 29 sites, and the effect on the reconstructed temperature change is also very small (mean $-2.46\text{ }^{\circ}\text{C}$ (-9.56 to $1.21\text{ }^{\circ}\text{C}$)). Thus, this sensitivity test shows that the influence of poor analogues in the LGM dataset is negligible and that the subtropical warming is robust.

Uncertainty. Because of the strong spatial autocorrelation in ocean temperatures, the uncertainty of the temperature prediction based on planktonic foraminifera assemblages is also spatially correlated. We have assessed the effect of the reconstruction uncertainty using a Monte Carlo approach. For each region, we generated 1,000 random temperature fields with the same spatial autocorrelation structure as the residuals of the transfer-function model. We added these to the reconstruction itself to determine the uncertainty in the overall estimated mean temperature change. Whenever multiple estimates were available for the same site, we reduced the uncertainty by the number of observations. The reconstruction errors (2 s.d.) vary regionally, with a median value of $1.52\text{ }^{\circ}\text{C}$. This uncertainty is larger than previously reported¹⁷ because our estimate accounts for spatial autocorrelation¹²⁰.

Anomalies. We present temperature anomalies with respect to climatology because not all LGM samples have a nearby core-top sample. Presenting anomalies with respect to temperature derived from the core-top assemblages would therefore result in reduced spatial coverage. We have nevertheless assessed whether the way the anomalies are calculated matters for the reconstructions by comparing the two different temperature anomalies for LGM sites with core-top samples within a 100 km radius. We find only a negligible and random difference ($0.01 \pm 1.27\text{ }^{\circ}\text{C}$; 1 s.d.) without any spatial pattern, validating the use of anomalies versus climatology.

Calculations. All calculations and visualizations were made in R¹²¹ using the packages tidyverse¹²², vegan¹²³, geosphere¹²⁴, patchwork¹²⁵, rioja¹²⁶, broom¹²⁷, fields¹²⁸, rgdal¹²⁹, sp^{130,131} and gstat^{132,133}. The reconstruction shown in Fig. 3 was gridded in an optimal way using the Data Interpolating Variational Analysis method¹³⁴ as outlined in ref. 135, but based on annual-mean sea-ice extent reconstruction and transfer-function results.

Data availability

The ForCenS core-top planktonic foraminifera compilation is available at <https://doi.org/10.1594/PANGAEA.873570> and the LGM assemblages can be accessed at <https://doi.org/10.5281/zenodo.10000129>. The foraminifera-based temperature are available at <https://doi.pangaea.de/10.1594/PANGAEA.962958>. The data PMIP simulation is available at the World Data Centre for Climate (<https://www.wdc-climate.de/ui/>). The DOIs for the individual simulations are provided in the references of Methods. Data from the simulations with the AWI-ESM can be found at <https://doi.org/10.5281/zenodo.8417872>.

Code availability

The code used for the analysis and visualization is available at https://github.com/lukasjonkers/LGM_forams.

References

- Siccha, M. & Kucera, M. ForCenS, a curated database of planktonic foraminifera census counts in marine surface sediment samples. *Sci. Data* **4**, 170109 (2017).
- Jonkers, L., Hillebrand, H. & Kucera, M. Global change drives modern plankton communities away from the pre-industrial state. *Nature* **570**, 372–375 (2019).
- Haslett, S. K. & Smart, C. W. Late Quaternary upwelling off tropical NW Africa: new micropalaeontological evidence from ODP Hole 658C. *J. Quat. Sci.* **21**, 259–269 (2006).
- de Garidel-Thoron, T. et al. A multiproxy assessment of the western equatorial Pacific hydrography during the last 30 kyr. *Paleoceanography* **22**, PA3204 (2007).
- Lopes dos Santos, R. A. et al. Comparison of organic ($\text{U}^{K_{37}}$, TEX^H_{86} , LDI) and faunal proxies (foraminiferal assemblages) for reconstruction of late Quaternary sea surface temperature variability from offshore southeastern Australia. *Paleoceanography* <https://doi.org/10.1002/palo.20035> (2013).
- Lessa, D. V. O., Santos, T. P., Venancio, I. M. & Albuquerque, A. L. S. Offshore expansion of the Brazilian coastal upwelling zones during Marine Isotope Stage 5. *Glob. Planet. Change* **158**, 13–20 (2017).
- Caley, T. et al. Quantitative estimate of the paleo-Agulhas leakage. *Geophys. Res. Lett.* **41**, 1238–1246 (2014).
- Voelker, A. H. L. & de Abreu, L. in *Abrupt Climate Change: Mechanisms, Patterns, and Impacts* Vol. 193 (eds Rashid, H. et al.) 15–37 (AGU, 2011).
- Hayward, B. W. et al. Planktic foraminifera-based sea-surface temperature record in the Tasman Sea and history of the Subtropical Front around New Zealand, over the last one million years. *Mar. Micropaleontol.* **82–83**, 13–27 (2012).
- Petró, S. M., Pivel, M. A. G., Coimbra, J. C. & Mizusaki, A. M. P. Paleooceanographic changes through the last 130 ka in the western South Atlantic based on planktonic Foraminifera. *Rev. Bras. Paleontol.* **19**, 3–14 (2016).
- Matsuzaki, K. M. R. et al. Paleoceanography of the Mauritanian margin during the last two climatic cycles: from planktonic foraminifera to African climate dynamics. *Mar. Micropaleontol.* **79**, 67–79 (2011).
- Arellano-Torres, E., Machain-Castillo, M. L., Contreras-Rosales, L. A., Cuesta-Castillo, L. B. & Ruiz-Fernández, A. C. Foraminiferal faunal evidence for glacial-interglacial variations in the ocean circulation and the upwelling of the Gulf of Tehuantepec (Mexico). *Mar. Micropaleontol.* **100**, 52–66 (2013).
- Naughton, F. et al. Wet to dry climatic trend in north-western Iberia within Heinrich events. *Earth Planet. Sci. Lett.* **284**, 329–342 (2009).
- Sánchez Goñi, M. F. et al. Contrasting impacts of Dansgaard-Oeschger events over a western European latitudinal transect modulated by orbital parameters. *Quat. Sci. Rev.* **27**, 1136–1151 (2008).
- Penard, A. et al. Contrasting paleoceanographic conditions off Morocco during Heinrich events (1 and 2) and the Last Glacial Maximum. *Quat. Sci. Rev.* **29**, 1923–1939 (2010).
- Chabaud, L., Sánchez Goñi, M. F., Desprat, S. & Rossignol, L. Land–sea climatic variability in the eastern North Atlantic subtropical region over the last 14,200 years: atmospheric and oceanic processes at different timescales. *Holocene* **24**, 787–797 (2014).
- Sanchez Goni, M. F., Bard, E., Landais, A., Rossignol, L. & d’Errico, F. Air–sea temperature decoupling in western Europe during the last interglacial–glacial transition. *Nat. Geosci.* **6**, 837–841 (2013).
- Xiang, R. et al. Planktonic foraminiferal records of East Asia monsoon changes in the southern South China Sea during the last 40,000 years. *Mar. Micropaleontol.* **73**, 1–13 (2009).
- Wary, M. et al. The southern Norwegian Sea during the last 45 ka: hydrographical reorganizations under changing ice-sheet dynamics. *J. Quat. Sci.* **32**, 908–922 (2017).
- Yu, P.-S. et al. Influences of extratropical water masses on equatorial Pacific cold tongue variability during the past 160 ka as revealed by faunal evidence of planktic foraminifera. *J. Quat. Sci.* **27**, 921–931 (2012).

58. Godad, S. P., Naidu, P. D. & Malmgren, B. A. Sea surface temperature changes during May and August in the western Arabian Sea over the last 22 kyr: implications as to shifting of the upwelling season. *Mar. Micropaleontol.* **78**, 25–29 (2011).
59. Crundwell, M., Scott, G., Naish, T. & Carter, L. Glacial–interglacial ocean climate variability from planktonic foraminifera during the mid-Pleistocene transition in the temperate Southwest Pacific, ODP Site 1123. *Palaeogeogr. Palaeoclimatol. Palaeoecol.* **260**, 202–229 (2008).
60. Steinke, S., Yu, P.-S., Kucera, M. & Chen, M.-T. No-analog planktonic foraminiferal faunas in the glacial southern South China Sea: implications for the magnitude of glacial cooling in the western Pacific warm pool. *Mar. Micropaleontol.* **66**, 71–90 (2008).
61. Wary, M. et al. Stratification of surface waters during the last glacial millennial climatic events: a key factor in subsurface and deep-water mass dynamics. *Clim. Past* **11**, 1507–1525 (2015).
62. Kuroyanagi, A., Kawahata, H., Narita, H., Ohkushi, K. & Aramaki, T. Reconstruction of paleoenvironmental changes based on the planktonic foraminiferal assemblages off Shimokita (Japan) in the northwestern North Pacific. *Glob. Planet. Change* **53**, 92–107 (2006).
63. Ijiri, A. et al. Paleoenvironmental changes in the northern area of the East China Sea during the past 42,000 years. *Palaeogeogr. Palaeoclimatol. Palaeoecol.* **219**, 239–261 (2005).
64. Ivanova, E. V., Beaufort, L., Vidal, L. & Kucera, M. Precession forcing of productivity in the Eastern Equatorial Pacific during the last glacial cycle. *Quat. Sci. Rev.* **40**, 64–77 (2012).
65. Carter, L., Manighetti, B., Ganssen, G. & Northcote, L. Southwest Pacific modulation of abrupt climate change during the Antarctic Cold Reversal–Younger Dryas. *Palaeogeogr. Palaeoclimatol. Palaeoecol.* **260**, 284–298 (2008).
66. Haddam, N. A. et al. Improving past sea surface temperature reconstructions from the Southern Hemisphere oceans using planktonic foraminiferal census data. *Paleoceanography* **31**, 822–837 (2016).
67. Haddam, N. A. et al. Changes in latitudinal sea surface temperature gradients along the Southern Chilean margin since the last glacial. *Quat. Sci. Rev.* **194**, 62–76 (2018).
68. Essallami, L., Sicre, M. A., Kallel, N., Labeyrie, L. & Siani, G. Hydrological changes in the Mediterranean Sea over the last 30,000 years. *Geochem. Geophys. Geosyst.* **8**, Q07002 (2007).
69. Sikes, E. L. et al. Southern Ocean seasonal temperature and Subtropical Front movement on the South Tasman Rise in the late Quaternary. *Paleoceanography* **24**, PA2201 (2009).
70. Ujiie, Y., Asahi, H., Sagawa, T. & Bassinot, F. Evolution of the North Pacific Subtropical Gyre during the past 190 kyr through the interaction of the Kuroshio Current with the surface and intermediate waters. *Paleoceanography* **31**, 1498–1513 (2016).
71. Simon, M. H. et al. Millennial-scale Agulhas Current variability and its implications for salt-leakage through the Indian–Atlantic Ocean Gateway. *Earth Planet. Sci. Lett.* **383**, 101–112 (2013).
72. Bostock, H. C., Hayward, B. W., Neil, H. L., Sabaa, A. T. & Scott, G. H. Changes in the position of the Subtropical Front south of New Zealand since the last glacial period. *Paleoceanography* **30**, 824–844 (2015).
73. Gebhardt, H. et al. Paleonutrient and productivity records from the subarctic North Pacific for Pleistocene glacial terminations I to V. *Paleoceanography* **23**, PA4212 (2008).
74. Mohtadi, M. & Hebbeln, D. Mechanisms and variations of the paleoproductivity off northern Chile (24°S–33°S) during the last 40,000 years. *Paleoceanography* **19**, PA2023 (2004).
75. Schulz, H. *Meeresoberflächentemperaturen vor 10.000 Jahren - Auswirkungen des frühholozänen Insolationseximums* (Geologisch-Paläontologisches Institut und Museum, 1995); <https://doi.org/10.2312/REPORTS-GPI.1995.73>
76. Martinez, J. I., Mora, G. & Barrows, T. T. Paleooceanographic conditions in the western Caribbean Sea for the last 560 kyr as inferred from planktonic foraminifera. *Mar. Micropaleontol.* **64**, 177–188 (2007).
77. Mix, A. C., Morey, A. E., Pisias, N. G. & Hostetler, S. W. Foraminiferal faunal estimates of paleotemperature: circumventing the no-analog problem yields cool Ice Age tropics. *Paleoceanography* **14**, 350–359 (1999).
78. Mix, A. C. & Morey, A. E. in *The South Atlantic* (eds Wefer, G. et al.) 503–525 (Springer, 1996).
79. Mohtadi, M., Steinke, S., Lückge, A., Groeneveld, J. & Hathorne, E. C. Glacial to Holocene surface hydrography of the tropical eastern Indian Ocean. *Earth Planet. Sci. Lett.* **292**, 89–97 (2010).
80. Setiawan, R. Y. et al. The consequences of opening the Sunda Strait on the hydrography of the eastern tropical Indian Ocean. *Paleoceanography* **30**, 1358–1372 (2015).
81. Mohtadi, M. et al. Glacial to Holocene swings of the Australian–Indonesian monsoon. *Nat. Geosci.* **4**, 540–544 (2011).
82. Gibbons, F. T. et al. Deglacial $\delta^{18}\text{O}$ and hydrologic variability in the tropical Pacific and Indian Oceans. *Earth Planet. Sci. Lett.* **387**, 240–251 (2014).
83. Romahn, S., Mackensen, A., Groeneveld, J. & Pätzold, J. Deglacial intermediate water reorganization: new evidence from the Indian Ocean. *Clim. Past* **10**, 293–303 (2014).
84. Voigt, I. et al. Variability in mid-depth ventilation of the western Atlantic Ocean during the last deglaciation: deglacial ventilation changes. *Paleoceanography* **32**, 948–965 (2017).
85. Howe, J. N. W. et al. Antarctic intermediate water circulation in the South Atlantic over the past 25,000 years: South Atlantic neodymium records. *Paleoceanography* **31**, 1302–1314 (2016).
86. Govin, A. et al. Terrigenous input off northern South America driven by changes in Amazonian climate and the North Brazil Current retroflection during the last 250 ka. *Clim. Past* **10**, 843–862 (2014).
87. Mohtadi, M. et al. North Atlantic forcing of tropical Indian Ocean climate. *Nature* **509**, 76–80 (2014).
88. Max, L. et al. Sea surface temperature variability and sea-ice extent in the subarctic northwest Pacific during the past 15,000 years. *Paleoceanography* **27**, PA3213 (2012).
89. Riethdorf, J.-R. et al. Millennial-scale variability of marine productivity and terrigenous matter supply in the western Bering Sea over the past 180 kyr. *Clim. Past* **9**, 1345–1373 (2013).
90. Hahn, A., Schefuß, E., Groeneveld, J., Miller, C. & Zabel, M. Glacial to interglacial climate variability in the southeastern African subtropics (25–20°S). *Clim. Past* **17**, 345–360 (2021).
91. Kucera, M., Rosell-Melé, A., Schneider, R., Waelbroeck, C. & Weinelt, M. Multiproxy approach for the reconstruction of the glacial ocean surface (MARGO). *Quat. Sci. Rev.* **24**, 813–819 (2005).
92. van Sebille, E. et al. Ocean currents generate large footprints in marine palaeoclimate proxies. *Nat. Commun.* **6**, 6521 (2015).
93. Von Gyldefeldt, A.-B., Carstens, J. & Meincke, J. Estimation of the catchment area of a sediment trap by means of current meters and foraminiferal tests. *Deep Sea Res.* **2** **47**, 1701–1717 (2000).
94. Antonov, J. I. *World Ocean Atlas 1998* Vol. 2 (NOAA, 1998); <https://psl.noaa.gov/data/gridded/data.nodc.woa98.html>
95. Gent, P. *CCSM4 Coupled Simulation for CMIP5 with Pre-industrial Forcings (1850), Served by ESGF* (WDCC, 2014); <https://doi.org/10.1594/WDCC/CMIP5.NRS4PC>
96. Otto-Bliessner, B. *CCSM4 Coupled Simulation for CMIP5 with Last Glacial Maximum Conditions, Served by ESGF* (WDCC, 2014); <https://doi.org/10.1594/WDCC/CMIP5.NRS4LG>
97. Sényesi, S. et al. *CNRM-CM5-2 Model Output Prepared for CMIP5 piControl, Served by ESGF* (WDCC, 2014); <https://doi.org/10.1594/WDCC/CMIP5.CEF5PC>

98. S n si, S. et al. *CNRM-CM5 Model Output Prepared for CMIP5 lgm*, Served by ESGF (WDCC, 2014); <https://doi.org/10.1594/WDCC/CMIP5.CEC5LG>
99. LASG, Institute of Atmospheric Physics, Chinese Academy of Sciences (IAP-LASG) *FGOALS-g2 Model Output Prepared for CMIP5 piControl*, Served by ESGF (WDCC, 2015); <https://doi.org/10.1594/WDCC/CMIP5.LSF2PC>
100. LASG, Institute of Atmospheric Physics, Chinese Academy of Sciences (IAP-LASG) *FGOALS-g2 Model Output Prepared for CMIP5 lgm*, Served by ESGF (WDCC, 2015); <https://doi.org/10.1594/WDCC/CMIP5.LSF2LG>
101. NASA Goddard Institute for Space Studies (NASA/GISS) *NASA-GISS: GISS-E2-R Model Output Prepared for CMIP5 Pre-industrial Control*, Served by ESGF (WDCC, 2014); <https://doi.org/10.1594/WDCC/CMIP5.GIGRpc>
102. NASA Goddard Institute for Space Studies (NASA/GISS) *NASA-GISS: GISS-E2-R Model Output Prepared for CMIP5 Last Glacial Maximum*, Served by ESGF (WDCC, 2014); <https://doi.org/10.1594/WDCC/CMIP5.GIGRlg>
103. Hajima, T. et al. *MIROC MIROC-ES2L Model Output Prepared for CMIP6 CMIP piControl* (ESGF, 2019); <https://doi.org/10.22033/ESGF/CMIP6.5710>
104. Ohgaito, R. et al. *MIROC MIROC-ES2L Model Output Prepared for CMIP6 PMIP lgm* (ESGF, 2019); <https://doi.org/10.22033/ESGF/CMIP6.5644>
105. Wieners, K.-H. et al. *MPI-M MPI-ESM1.2-LR Model Output Prepared for CMIP6 CMIP piControl* (ESGF, 2019); <https://doi.org/10.22033/ESGF/CMIP6.6675>
106. Jungclaus, J. et al. *MPI-M MPI-ESM1.2-LR Model Output Prepared for CMIP6 PMIP lgm* (ESGF, 2019); <https://doi.org/10.22033/ESGF/CMIP6.6642>
107. Yukimoto, S. et al. *MRI-CGCM3 Model Output Prepared for CMIP5 piControl*, Served by ESGF (WDCC, 2015); <https://doi.org/10.1594/WDCC/CMIP5.MRMCPc>
108. Yukimoto, S. et al. *MRI-CGCM3 Model Output Prepared for CMIP5 lgm*, Served by ESGF (WDCC, 2015); <https://doi.org/10.1594/WDCC/CMIP5.MRMCLG>
109. Kageyama, M. et al. The PMIP4 contribution to CMIP6—part 4: scientific objectives and experimental design of the PMIP4-CMIP5 Last Glacial Maximum experiments and PMIP4 sensitivity experiments. *Geosci. Model Dev.* **10**, 4035–4055 (2017).
110. Abe-Ouchi, A. et al. Ice-sheet configuration in the CMIP5/PMIP3 Last Glacial Maximum experiments. *Geosci. Model Dev.* **8**, 3621–3637 (2015).
111. Anderson, P. M., Bartlein, P. J., Brubaker, L. B., Gajewski, K. & Ritchie, J. C. Modern analogues of late-Quaternary pollen spectra from the western interior of North America. *J. Biogeogr.* **16**, 573–596 (1989).
112. Bray, J. R. & Curtis, J. T. An ordination of the upland forest communities of southern Wisconsin. *Ecol. Monogr.* **27**, 325–349 (1957).
113. Anderson, M. J. et al. Navigating the multiple meanings of β diversity: a roadmap for the practicing ecologist. *Ecol. Lett.* **14**, 19–28 (2011).
114. Neukom, R., Steiger, N., G mez-Navarro, J. J., Wang, J. & Werner, J. P. No evidence for globally coherent warm and cold periods over the preindustrial Common Era. *Nature* **571**, 550–554 (2019).
115. B , A. W. H. & Tolderlund, D. S. in *The Micropaleontology of Oceans* (eds Funnell, B. M. & Riedel, W. R.) 105–149 (Cambridge Univ. Press, 1971).
116. Prell, W. *Stability of Low-Latitude Sea-Surface Temperatures: An Evaluation of the CLIMAP Reconstruction with Emphasis on the Positive SST Anomalies* (DOE, 1985).
117. Telford, R. J. & Birks, H. J. B. A novel method for assessing the statistical significance of quantitative reconstructions inferred from biotic assemblages. *Quat. Sci. Rev.* **30**, 1272–1278 (2011).
118. Jonkers, L. & Ku era, M. Global analysis of seasonality in the shell flux of extant planktonic foraminifera. *Biogeosciences* **12**, 2207–2226 (2015).
119. Rebotim, A. et al. Factors controlling the depth habitat of planktonic foraminifera in the subtropical eastern North Atlantic. *Biogeosciences* **14**, 827–859 (2017).
120. Telford, R. J. & Birks, H. J. B. Evaluation of transfer functions in spatially structured environments. *Quat. Sci. Rev.* **28**, 1309–1316 (2009).
121. R Core Team *R: A Language and Environment for Statistical Computing* (R Foundation for Statistical Computing, 2020); <https://www.R-project.org/>
122. Wickham, H. et al. Welcome to the tidyverse. *J. Open Source Softw.* **4**, 1686 (2019).
123. Oksanen, J. et al. *vegan: Community Ecology Package* (CRAN.R-project, 2020); <https://CRAN.R-project.org/package=vegan>
124. Hijmans, R. J. *geosphere: Spherical Trigonometry* (CRAN.R-project, 2019); <https://CRAN.R-project.org/package=geosphere>
125. Pedersen, T. L. *patchwork: The Composer of Plots* (CRAN.R-project, 2020); <https://CRAN.R-project.org/package=patchwork>
126. Juggins, S. *rioja: Analysis of Quaternary Science Data* (CRAN.R-project, 2020); <https://cran.r-project.org/package=rioja>
127. Robinson, D., Hayes, A. & Couch, S. *broom: Convert Statistical Objects into Tidy Tibbles* (CRAN.R-project, 2021); <https://CRAN.R-project.org/package=broom>
128. Nychka, D., Furrer, R., Paige, J. & Sain, S. *fields: Tools for Spatial Data* (UCAR, 2017); <https://doi.org/10.5065/D6W957CT>
129. Bivand, R., Keitt, T. & Rowlingson, B. *rgdal: Bindings for the 'Geospatial' Data Abstraction Library* (CRAN.R-project, 2021); <https://CRAN.R-project.org/package=rgdal>
130. Pebesma, E. J. & Bivand, R. S. Classes and methods for spatial data in R. *R News* **5**, 9–13 (2005).
131. Bivand, R. S., Pebesma, E. J., G mez-Rubio, V. & Pebesma, E. J. *Applied Spatial Data Analysis with R* (Springer, 2013).
132. Pebesma, E. J. Multivariable geostatistics in S: the gstat package. *Comput. Geosci.* **30**, 683–691 (2004).
133. Gr ler, B., Pebesma, E. & Heuvelink, G. Spatio-temporal interpolation using gstat. *R J.* **8**, 204–218 (2016).
134. Troupin, C. et al. Generation of analysis and consistent error fields using the Data Interpolating Variational Analysis (DIVA). *Ocean Model.* **52–53**, 90–101 (2012).
135. Paul, A., Multiza, S., Stein, R. & Werner, M. A global climatology of the ocean surface during the Last Glacial Maximum mapped on a regular grid (GLOMAP). *Clim. Past* **17**, 805–824 (2021).

Acknowledgements

This work was supported by the German Federal Ministry of Education and Research (BMBF) as a Research for Sustainability initiative (FONA); through the PALMOD project (grant nos. O1LP1922A LJ, O1LP1924B XS and O1LP1509C AMD) and through the Cluster of Excellence, The Ocean Floor—Earth’s Uncharted Interface funded by the German Research Foundation (DFG; EXC 2077, grant no. 390741603 MCR). We also acknowledge funding from the European Research Council (ERC) under the European Union’s Horizon 2020 research and innovation programme (grant agreement no. 716092 TL) and the National Natural Science Foundation of China (NSFC) (grant no. 42206256 XS). The hosing simulations with the AWI-ESM were conducted on the AWI supercomputer (Ollie). We thank all researchers who shared LGM assemblage data and R. Telford for helpful discussions. Sample material has been provided by the GeoB Core Repository at the MARUM—Center for Marine Environmental Sciences, University of Bremen, Germany. We acknowledge the World Climate Research Programme’s Working Group on Coupled Modelling, which is responsible for CMIP, and we thank the climate modelling groups for producing and making available their model output. For CMIP, the US Department of Energy’s Program for Climate Model Diagnosis and

Intercomparison provides coordinating support and led development of software infrastructure in partnership with the Global Organization for Earth System Science Portals.

Author contributions

This study was conceptualized by L.J. and M.K. L.J. and T.L. curated the data. L.J. and M.C.R. designed the methodology. The formal analysis was done by L.J. with contributions by X.S. and A.P. Investigation of the results was carried out by L.J. and X.S. M.K. was responsible for funding acquisition. L.J. created the visualization and prepared and wrote the original draft. L.J., T.L., M.C.R., X.S., A.M.D., G.L., A.P., A.M. and M.K. reviewed and edited the paper.

Funding

Open access funding provided by Staats- und Universitätsbibliothek Bremen.

Competing interests

The authors declare no competing interests.

Additional information

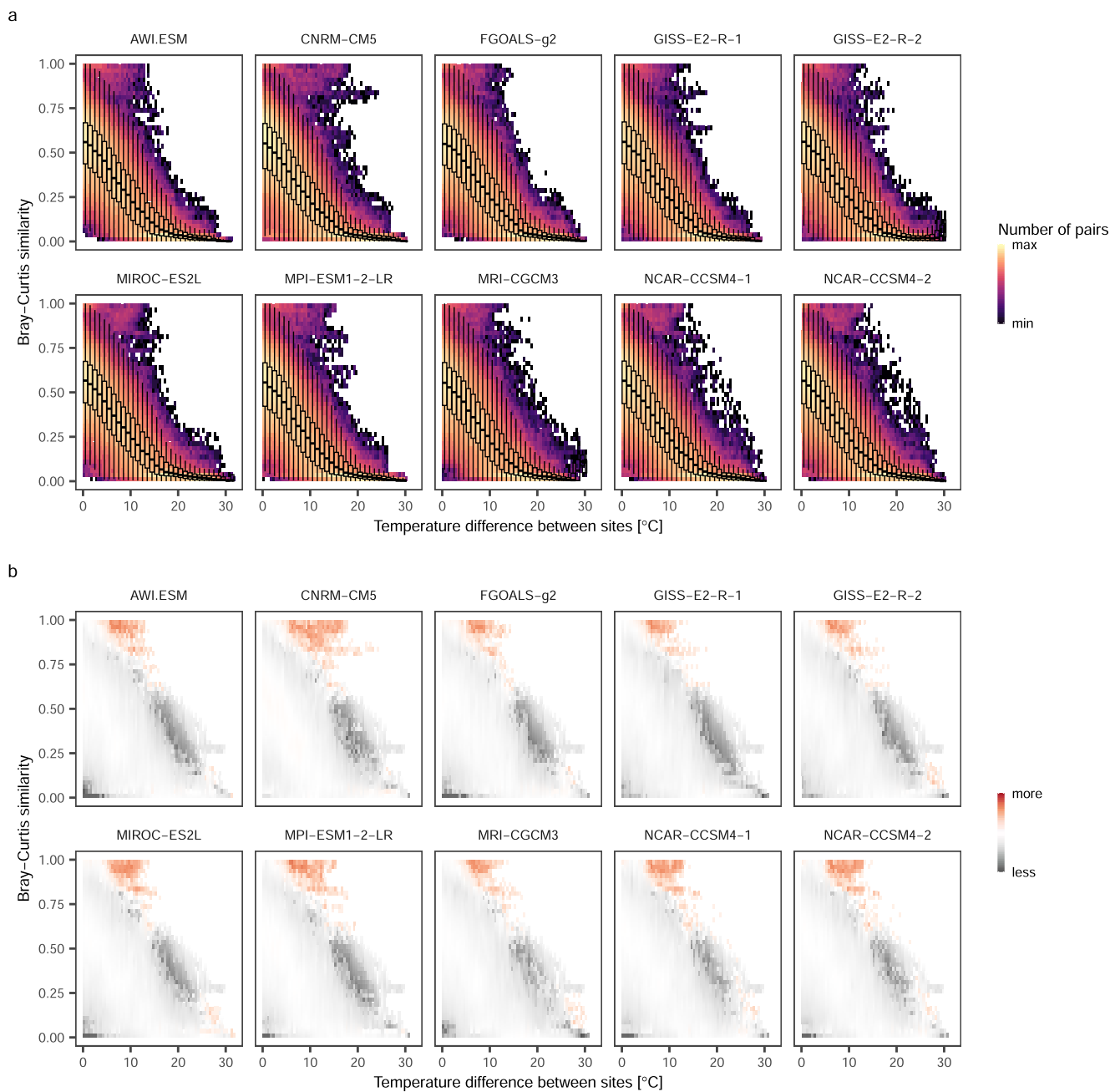
Extended data is available for this paper at <https://doi.org/10.1038/s41561-023-01328-7>.

Supplementary information The online version contains supplementary material available at <https://doi.org/10.1038/s41561-023-01328-7>.

Correspondence and requests for materials should be addressed to Lukas Jonkers.

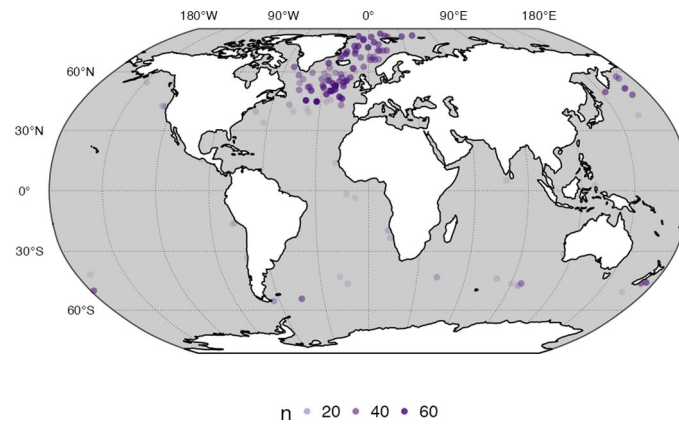
Peer review information *Nature Geoscience* thanks Tracy Aze, Marci Robinson and Adam Woodhouse for their contribution to the peer review of this work. Primary Handling Editors: James Super and Alison Hunt, in collaboration with the *Nature Geoscience* team.

Reprints and permissions information is available at www.nature.com/reprints.



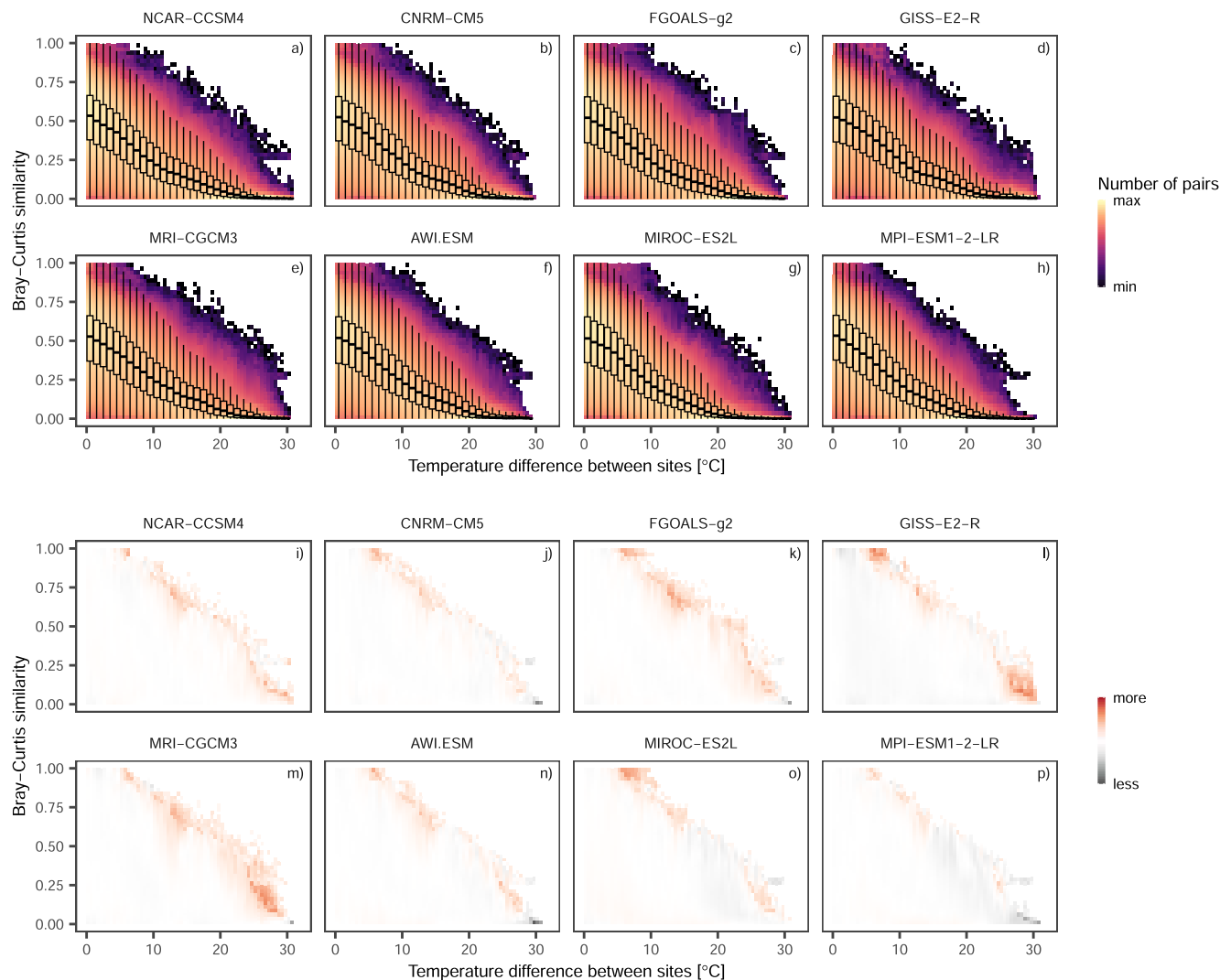
Extended Data Fig. 1 | LGM similarity decay patterns for individual model simulations. Panel a shows the similarity-decay patterns based on simulated LGM temperatures and b the difference from the modern pattern (Fig. 2a). Note the presence of samples with high similarities (above 0.75) at large environmental

distances (around 10 °C) that characterises all simulations and is inconsistent with the modern distance-decay pattern. Box-plots indicate the median and interquartile range of the data; the whiskers extend to 1.5 times this range.



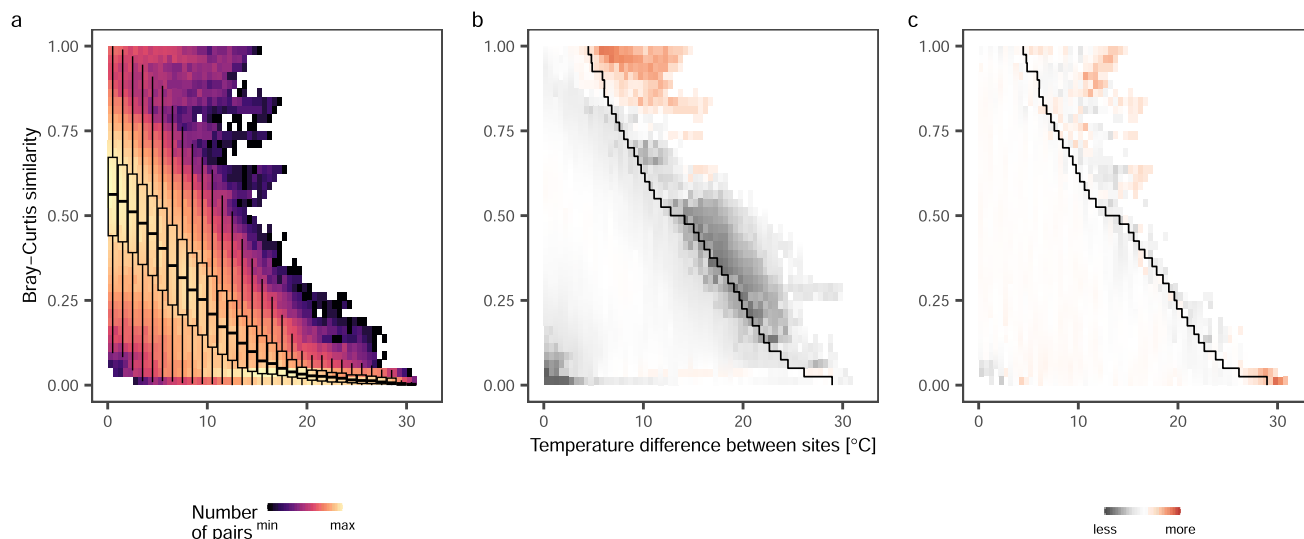
Extended Data Fig. 2 | Spatial origin of the anomalous LGM similarity decay pattern. Spatial distribution of the site pairs that show high similarity at large simulated thermal differences (the area in red in Fig. 2c). Transparency of the

dots indicates in how many pairs the site occurs. The distribution of these sites with similar species assemblages is consistent with the distribution of the cold-water assemblages during the LGM (Fig. 1). Map made with Natural Earth.



Extended Data Fig. 3 | Similarity decay pattern based on simulated pre-industrial temperatures. Modern (core top) similarity-decay patterns based on simulated pre-industrial temperatures from each simulation (**a–h**) and the difference from the reference similarity decay using climatology (**i–p**). The decay using simulated temperatures is largely similar to the decay obtained when using

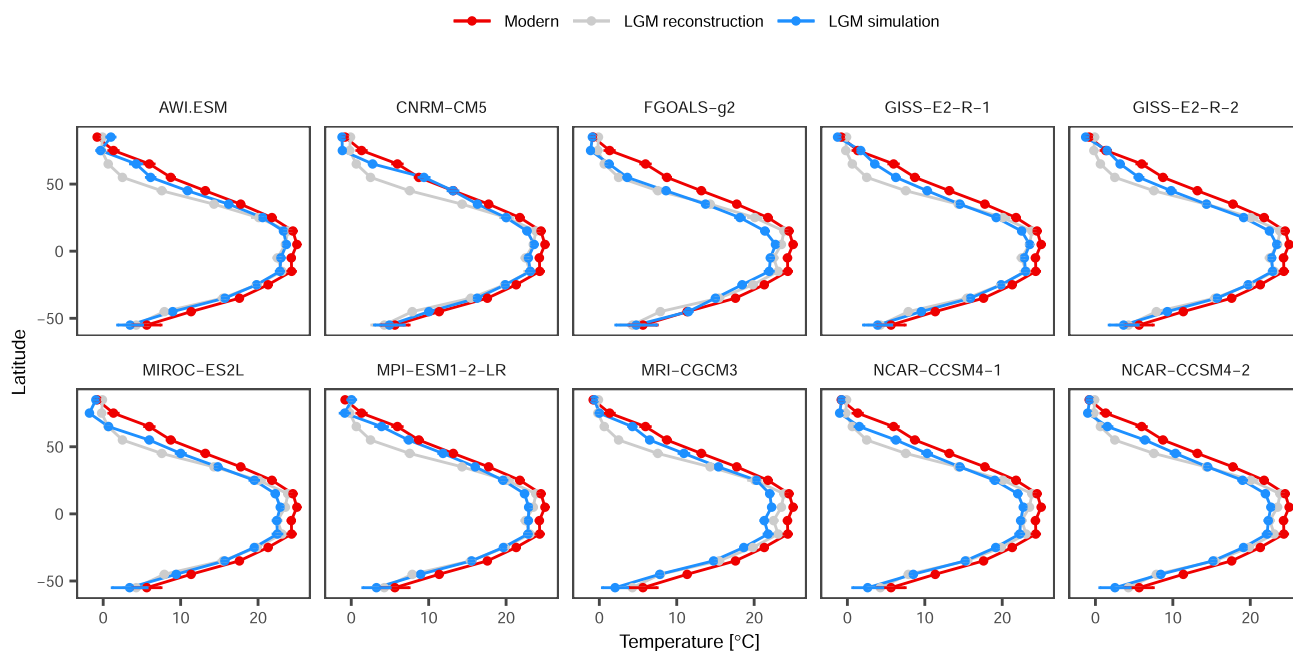
climatology, indicating that the anomalous similarity-decay pattern using LGM simulations is not related to overall model bias, but reflects the simulated LGM temperature pattern. Box-plots indicate the median and interquartile range of the data; the whiskers extend to 1.5 times this range.



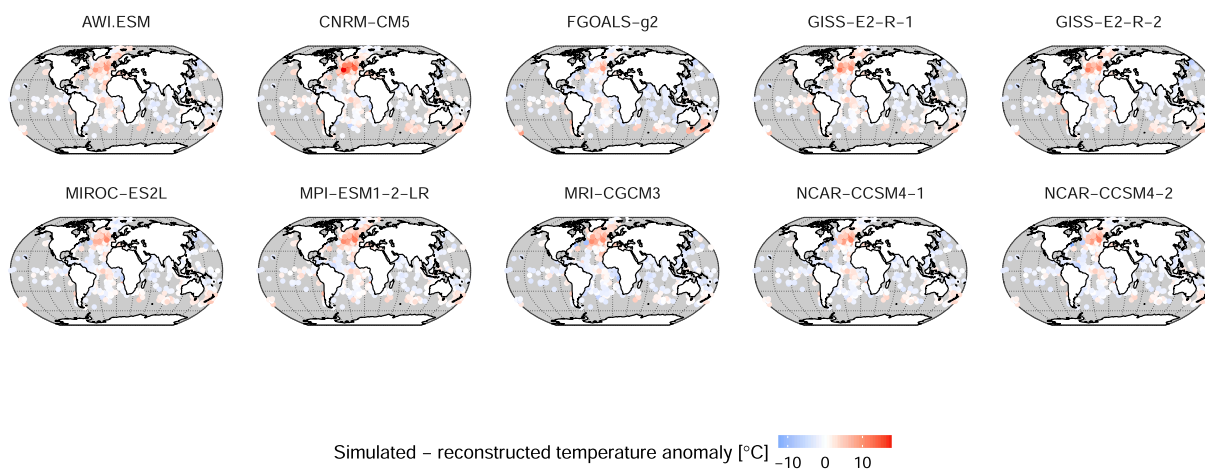
Extended Data Fig. 4 | Ecological evidence that the simulated glacial cooling is too uniform. The similarity decay pattern obtained using LGM assemblages and modern temperatures (a) also shows the existence of nearly identical species assemblages at large thermal differences that characterises the pattern obtained using simulated LGM temperatures (compare to Fig. 2b). The resulting difference from the core top pattern (b) also differs only marginally from the pattern obtained using simulated LGM temperatures (compare to Fig. 2c). Panel c shows the difference between the decay pattern obtained from LGM

assemblages and using modern temperature (panel a in this figure) and using simulated LGM temperatures (Fig. 2b). The fact that the similarity decay patterns are nearly identical indicates that the simulated LGM temperature field is merely offset from the modern by a globally constant amount, whereas the species assemblages indicate marked spatial differences in the cooling and fundamental changes in the oceanic thermal gradients. Box-plots in a indicate the median and interquartile range of the data; the whiskers extend to 1.5 times this range.

a

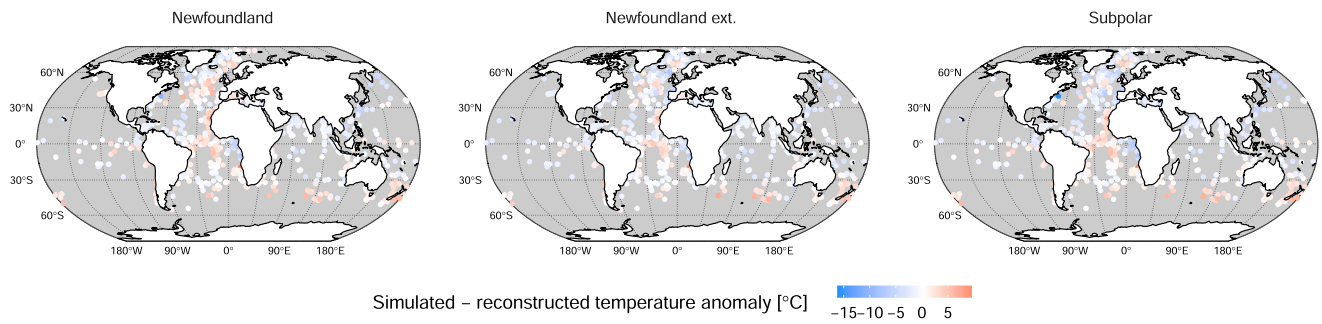


b

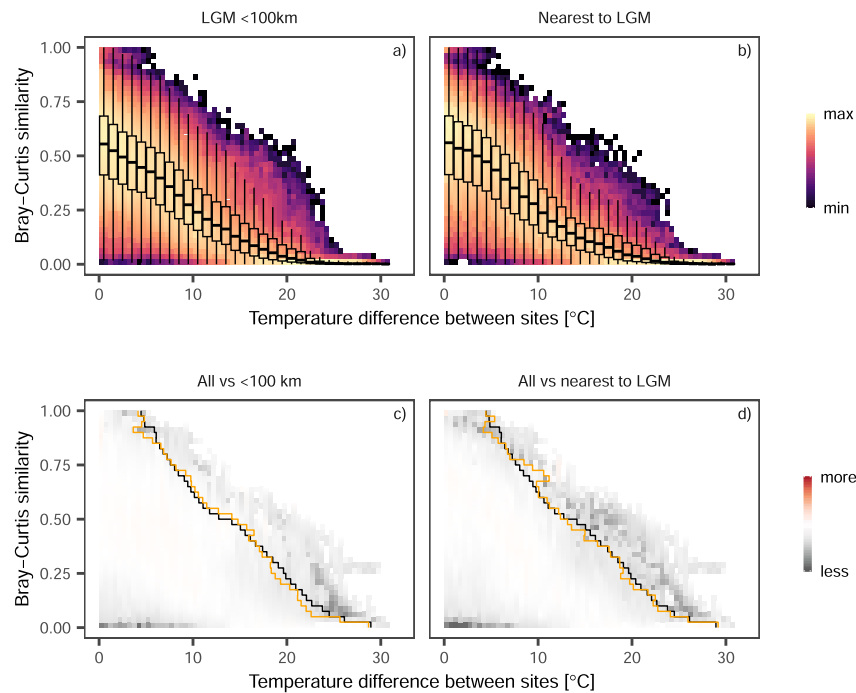


Extended Data Fig. 5 | Comparing reconstructed and simulated seawater temperatures. **a)** latitudinal patterns. In almost all cases, the simulated LGM temperature pattern is similar to the modern pattern, whereas the foraminifera-based LGM reconstruction indicates that the gradient in the Northern hemisphere was much steeper, and that the contrast between high and mid latitudes was reduced. The reduction in the thermal contrast between the high and mid northern latitudes is also visible in the similarity-decay pattern (Fig. 2).

All comparisons are carried out at the sites of the reconstruction; dots represent averages of 10° bins; error bars, mostly hidden behind the dots, are standard errors of the mean. **b)** difference between simulated and reconstructed LGM temperature anomalies in the equilibrium simulations. The overall pattern is similar for all models, with the greatest difference observed in the midlatitude North Atlantic Ocean; however, the magnitude of the difference varies by model. Maps made with Natural Earth.

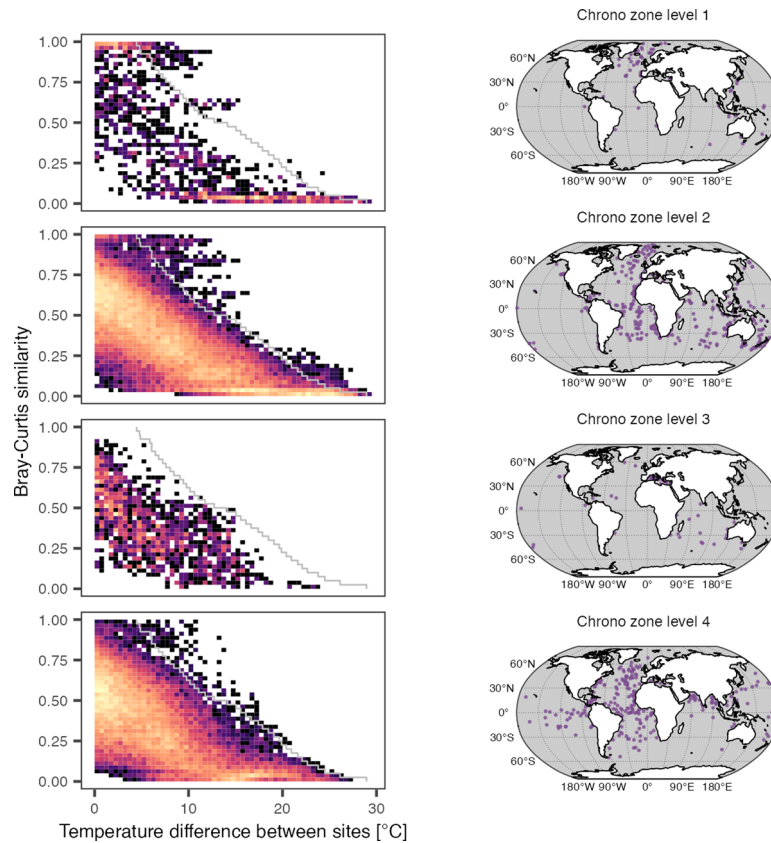


Extended Data Fig. 6 | Difference between simulated and reconstructed LGM temperature anomalies in the simulations with an additional freshwater flux into the North Atlantic. Headers refer to the different experiments where freshwater forcing was applied for different durations to different location, for details see Methods. Maps made with Natural Earth.



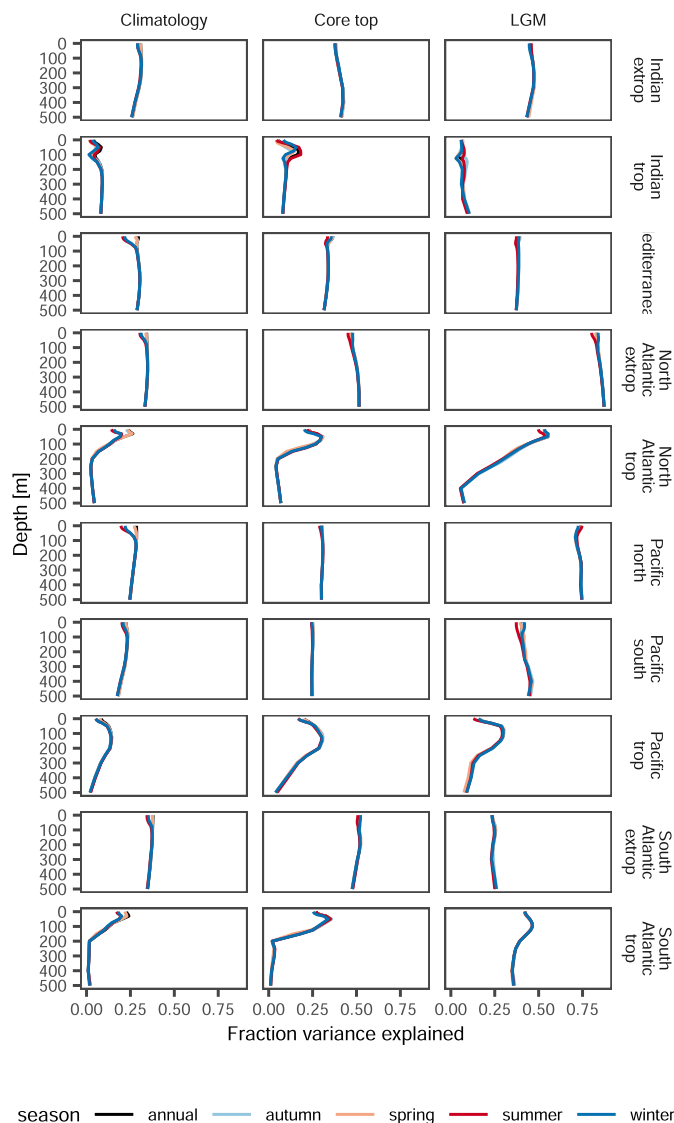
Extended Data Fig. 7 | The modern similarity decay pattern is robust and not an artefact of the sampling distribution. The plots are like Fig. 2, showing the pairwise similarity for all samples; brighter colours indicate higher density of pairs between which the environmental and community distance is determined. Box-whisker plots highlight the general similarity decay pattern and show the median and interquartile range of the data; the whiskers extend to 1.5 times this range. The pattern in the entire core top data set is nearly identical to that in the core top samples that are within 100 km of an LGM sample (a), as well as the pattern in the core top samples closest to the LGM samples (b). Importantly,

the cluster of LGM assemblage pairs with high similarity at large simulated temperature distances visible in Fig. 2 is absent here in both subsets. Note also that the differences between the subsets of the modern core top samples (c, d) are smaller than the differences between the core top pattern and the LGM pattern using simulated temperatures (Fig. 2). The step lines in c and d show the 99th percentile of the temperature differences across the similarity range (black for the entire dataset (as in Fig. 2) and orange for the subset). The small differences show that there is negligible effect of subsetting the core top data on the assemblage limits.



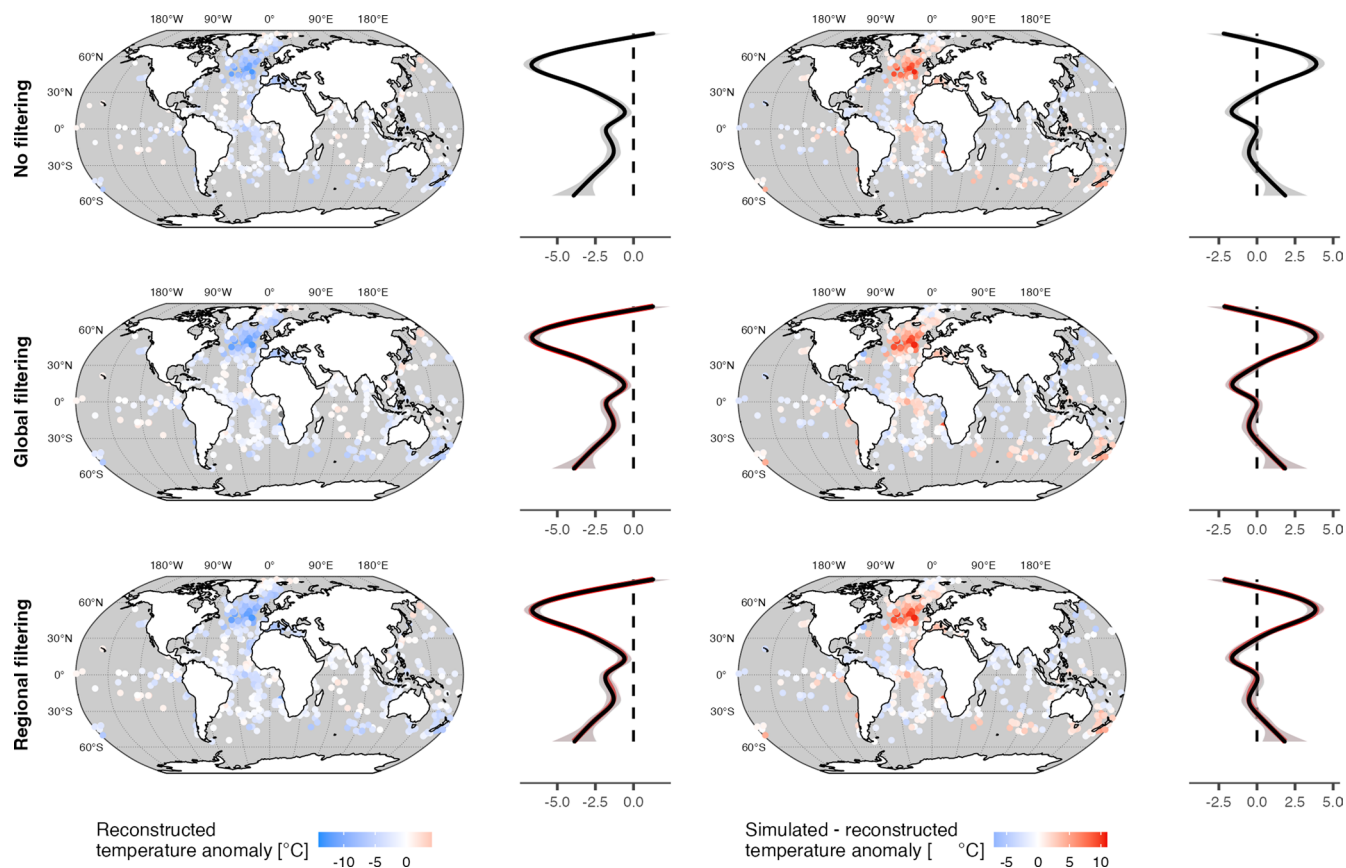
Extended Data Fig. 8 | Sensitivity of the similarity decay pattern among LGM planktonic foraminifera to chronological control. Chronological control decreases from 1–3; level 4 indicates legacy samples for which too little information is available to establish chronological robustness (see details in

Methods). Importantly, the anomalously high similarities at large temperature gradients are formed by samples with high chronological confidence. The pattern is therefore likely robust against age uncertainty. Maps made with Natural Earth.



Extended Data Fig. 9 | Transfer function model attribution. Temperatures, either observed (Climatology) or predicted (Core top, LGM), that explain most of the variance in the core top and in the LGM planktonic foraminifera assemblages are likely to be the best candidates for reconstruction. The graphs show the fraction of variance in the planktonic foraminifera assemblages that is explained by temperature at different times of the year (colours) and at different depths in the water column. Left column: results from CCA using core-top assemblage data and climatology temperature data; middle column: variance explained by the core-top data (Modern) and temperatures predicted using transfer

functions; right column: species variance in the LGM data set explained by the foraminifera-based reconstructions. These analyses show that temperatures from all seasons explain approximately the same amount of planktonic foraminifera assemblage variability in all regions. However, there are marked differences in the amount of variance explained by temperatures at different depths. The sensitivity to depth is higher in the tropics, consistent with the larger vertical temperature gradients. Globally, most of the variance in the planktonic foraminifera assemblages is explained by annual-mean temperatures at 50 m water depth.



Extended Data Fig. 10 | The reconstructed temperature pattern based on planktonic foraminifera assemblages is not affected by poor analogues in the LGM dataset. The left-hand column shows the reconstructed temperature anomalies and the black lines indicate the latitudinal patterns; the right-hand column shows the difference between the mean simulated and the reconstructed temperature anomalies. Top row is the reconstruction shown in the main text

without analogue filtering. The rows below show the data with global and regional analogues filtering (Methods), respectively. The latitudinal pattern of the complete dataset (top row) is plotted in red in the panels below, but remains almost invisible because of the overlap. Note that the slight warming at many low latitude sites and in the Pacific is not an artefact of poor analogues. Maps made with Natural Earth.